CrossMark

Retired A Stars and Their Companions. VIII. 15 New Planetary Signals around Subgiants and Transit Parameters for California Planet Search Planets with Subgiant Hosts

Jacob K. Luhn[1,5] , Fabienne A. Bastien[1] , Jason T. Wright[1] , John A. Johnson[2], Andrew W. Howard[3] , and Howard Isaacson[4]

[1] Department of Astronomy, The Pennsylvania State University, 525 Davey Lab, University Park, PA 16802, USA; jluhn@psu.edu
[2] Institute for Theory and Computation, Harvard-Smithsonian Center for Astrophysics, 60 Garden Street, Cambridge, MA 02138, USA
[3] Department of Astronomy, California Institute of Technology, Pasadena, CA, USA
[4] Astronomy Department, University of California, Berkeley, CA, USA

Abstract

We present the discovery of seven new planets and eight planet candidates around subgiant stars, as additions to the known sample of planets around "retired A stars." Among these are the possible first three-planet systems around subgiant stars, HD 163607 and HD 4917. Additionally, we present calculations of possible transit times, durations, depths, and probabilities for all known planets around subgiant ($3 < \log g < 4$) stars, focused on possible transits during the *TESS* mission. While most have transit probabilities of 1%–2%, we find that there are three planets with transit probabilities >9%.

Key words: planets and satellites: detection – planets and satellites: fundamental parameters – techniques: radial velocities

Supporting material: machine-readable tables

1. Introduction

The occurrence rate of Jupiter-mass planets has been observed to increase with both metallicity and mass of the host star (Ida & Lin 2004; Fischer & Valenti 2005; Bowler et al. 2010; Johnson et al. 2010a). Despite the increased occurrence rates, more massive stars show a paucity in the number of massive planets at short periods, both "hot Jupiters" on very close orbits and even those out to separations of ∼1 au (Johnson et al. 2007a; Sato et al. 2008). As these planets are the easiest to detect via radial velocity (RV) and transit photometry methods, this does not represent an observational bias, indicating that stellar mass plays a large role in shaping the formation and orbital evolution of planets.

Johnson et al. (2006) targeted intermediate-mass evolved stars in an effort to observe and study the properties of planets around stars more massive than the Sun. The stars selected for the survey come from just below a section of the main sequence known as the Hertzsprung gap (HG), which lies between the main sequence and the red giant branch. The sample was selected to include mostly intermediate-mass stars ($M_\star \gtrsim 1.3\,M_\odot$), often referred to as "retired A-type" stars because they had A spectral types when they were on the main sequence. On the main sequence, these stars are difficult targets for precise RV measurements for two reasons: first, because they rotate rapidly, any absorption features they have are significantly Doppler-broadened and, second, because of their high effective temperatures, they lack strong absorption lines observed in cooler stars. As a result, typical RV surveys avoid main-sequence stars with intermediate to high masses. However, stars of this mass that have left the main sequence become suitable for RV measurements due to their cooler atmospheres and slower rotational velocities, which lead to narrower absorption features in their spectra. The Retired A-star survey

has been responsible for the discovery of more than 40 exoplanets around subgiant stars to date.[6]

The planets discovered by the Retired A-star survey exhibit two key differences from planets discovered around lower mass main-sequence stars: (1) an increased abundance of giant planets and (2) a decrease in planets with shorter periods. These differences between the planets around more massive stars and those on the main sequence has sparked debate about the true masses of the stars themselves (Lloyd 2011, 2013; Johnson et al. 2013; Johnson & Wright 2013). The essence of the debate revolves around the statistical likelihood of finding a large population of relatively massive stars in the region of the HR diagram selected for the Retired A-star survey. Different galactic models and using volume-limited versus magnitude-limited samples produce conflicting results for the expected number of massive stars. Furthermore, Schlaufman & Winn (2013) investigated the kinematics of these stars, concluding that the velocity dispersions were too high for them to in fact be massive stars. Using asteroseismology, Stello et al. (2017) showed that there was indeed an overestimate in mass for stars above $1.6\,M_\odot$ among their sample of eight stars. More recently, Ghezzi et al. (2018) reanalyzed a subset of the Retired A Star sample and determined atmospheric, rotational, evolutionary, and kinematic parameters, finding errors much lower than the 50% overestimate suggested by Lloyd (2011, 2013). By accounting for reddening, they find that the velocity dispersions are consistent with those of more massive main-sequence stars with an offset of $0.04\,M_\odot$, suggesting that these are in fact massive stars. Putting aside the mass argument, because the Retired A-star sample is composed of entirely evolved stars,[7] the "desert" of short-period planets appears regardless of the true mass of these stars, as there is a noticeable lack of short-period planets around post-main-sequence stars. In fact, there appears to be a pileup of

---

[6] http://exoplanets.org

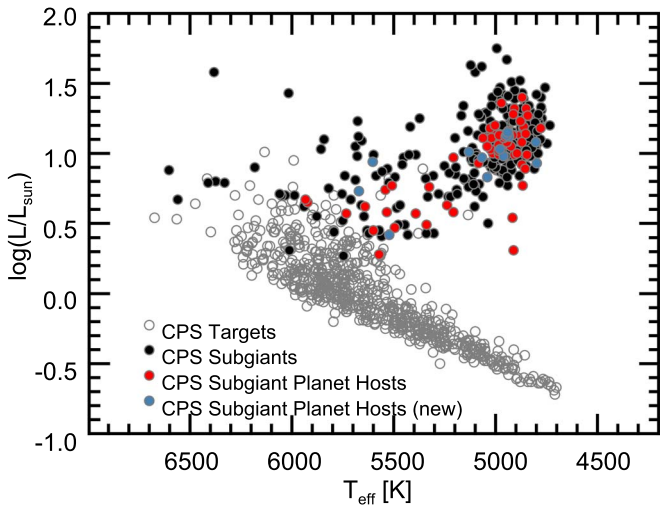[7] Selected based on their position near the Hertzsprung gap.

Figure 1. HR diagram showing the sample of subgiants among all CPS stars and the subset of those that are planet-host stars. All CPS target stars with $T_{\rm eff}$ and $\log(L/L_\odot)$ values from Brewer et al. (2016) are shown in gray. The black points show the subsample of CPS subgiant stars, which are here chosen to be stars with $3.0 < \log g < 4.0$. The planet-host stars (known and new in this work) are shown in red.

planets around post-main-sequence stars at 1–2 au, all with masses $\sim$1–5 $M_{\rm Jup}$, possibly indicating that these types of planets are those most likely to remain after post-main-sequence stellar evolution while most planets interior to this region are lost due to tidal capture (Villaver & Livio 2009).

Given the lack of short-period planets around subgiants, there are few planets around subgiants that are easily detectable by transit surveys. Despite this, a handful of short-period planets with subgiant hosts have been discovered by *Kepler* (Borucki et al. 2010), namely *Kepler* 435 b (Borucki et al. 2010); *Kepler* 56 b,c (Borucki et al. 2011); *Kepler* 108 b,c, 278 b,c, 391 b,c (Rowe et al. 2014); *Kepler* 432 b (Ciceri et al. 2015); and *Kepler* 637 b, 815 b, 1270 b, 774 b, 1004 b, 1394 b, and 643 b (Morton et al. 2016) as well as one planet in the KELT survey, KELT-11 b (Pepper et al. 2017).[8] Unfortunately, the *Kepler* subgiants are generally too faint and were lower priority than dwarfs for RV follow-up and so we do not have measured masses for most of these planets.[9] However, given the large sample of existing RV subgiants with known planets, we have the opportunity to examine the transit probabilities for these lower priority transit search targets, in the context of future transit surveys, particularly on the upcoming *TESS* mission (Ricker et al. 2014). Observing transits of existing RV planets has a number of advantages, the biggest being removing the $\sin i$ degeneracy for the masses of these planets. Additionally, transits provide a model-independent measure of the stellar density, which could be useful for confirming the masses of the host stars. Another benefit is the tendency of RV surveys to target bright stars, which enables easier ground-based follow-up and provides targets for transmission spectroscopy, for which we have very few studies of temperate, long-period Jupiter-sized planets (Kane et al. 2009). Despite large transit surveys (KELT, HAT, *Kepler*, *K2*) in this time, long-period Jupiters with hosts bright enough for transmission spectroscopy remain scarce. With

these ideas in mind, we present transit parameters for subgiant stars already observed by the California Planet Search (CPS; Howard et al. 2010) RV survey.

In Section 2, we describe our sample of subgiant stars, RV measurements, and stellar properties. We then present the discovery of 15 new planetary signals around subgiant stars and several stellar companions, spanning a spectrum of secure detections. Section 3 contains those that we determine to be secure planet detections. Section 4 lists those that are "planet candidates" to better illustrate the varying degrees of security. We include all probable planet candidates in the interest of listing the possible transit times for planets around subgiant hosts. Section 5 contains a list of the stellar companions. The new planetary signals in this work increase the sample of RV planets around subgiants by more than 25%. In Section 6 we present the transit parameters for these stars. Despite the typically small transit probability of 1%–2%, it is likely, given the sample size of 85 planets, that several do indeed transit. Finally, we present a summary and our conclusion in Section 7.

2. Observations

2.1. Sample Selection and Stellar Properties

Our sample is composed of stars observed as part of the CPS with $3.0 < \log g < 4.0$. From this sample of over 400 stars, we have identified those that are known to host planets, as identified in either www.exoplanets.org or www.exoplanet.eu. This list comprises 42 stars in our sample. Figure 1 shows an HR diagram of the entire CPS sample, the subset of CPS subgiant stars, and the planet-host stars in our sample.

All stellar properties come from Brewer et al. (2016; erratum Brewer et al. 2017 cited as B17 hereafter), who used one-dimensional LTE model spectra to fit to a star's observed spectrum to determine effective temperatures, metallicities, surface gravities, and elemental abundances. In conjunction with *Hipparcos* parallaxes and *V*-band magnitudes, these spectral measurements were used to derive masses, radii, and luminosities. Their iterative fitting technique and improved line list correct for systematic discrepancies in $\log g$ between spectroscopy and asteroseismology (Huber et al. 2013; Bastien et al. 2014) and their spectroscopic methods are now consistent with the values of $\log g$ obtained from asteroseismology (Brewer et al. 2015). The stellar properties for the stars in this sample are given in Table 2. We note that while Ghezzi et al. (2018) determined masses and radii with smaller uncertainties than Brewer et al. (2016) for a subset of the Retired A sample, more than 25% of the stars in this work were not reanalyzed by Ghezzi et al. (2018). Since the stellar parameters are largely consistent within errors between Ghezzi et al. (2018) and Brewer et al. (2016), we use stellar properties from Brewer et al. (2016) for consistency.[10]

2.2. Spectra and RV Measurements

Observations were taken at Keck Observatory using the High Resolution Echelle Spectrometer (HIRES) with a resolution of

---

[8] KELT-6 b (Collins et al. 2014) also orbits what appears to be a very slightly evolved subgiant.

[9] Those with measured masses are *Kepler* 56 b,c (Otor et al. 2016) and *Kepler* 432 c (Quinn et al. 2015).

---

[10] The radius measurement of HD 193342 is the only parameter for which the two samples are not consistent within the errors, with radius 6 $R_\odot$ from Brewer et al. (2016) and 8.5 $R_\odot$ from Ghezzi et al. (2018). Despite this large discrepancy, the radius difference will only affect the predicted transit parameters for HD 193342 b, which is unlikely to transit (0.27% transit probability). Using the radius from Ghezzi et al. (2018) would result in a slightly increased transit probability ($\sim$0.4%) as well as a smaller transit depth and longer transit durations if it does indeed transit.

Table 1
Summary of Additional Non-Keck HIRES Velocities

Star	Telescope	Instrument	N_{obs}	References
HD 1502	Harlan J. Smith Telescope	TCS	25	Johnson et al. (2011)
HD 1502	Hobby–Eberly Telescope	HRS	20	Johnson et al. (2011)
HD 159868	Anglo-Australian Telescope	UCLES	47	Wittenmyer et al. (2012)
HD 192699	Lick Observatory	Hamilton spectrometer	34	Johnson et al. (2007b)
HD 114613	Anglo-Australian Telescope	UCLES	222	Wittenmyer et al. (2014)
HD 38801	Subaru	High Dispersion Spectrograph	11	Harakawa et al. (2010)
HD 181342	CTIAO 1.5 m	CHIRON	11	Jones et al. (2016)
HD 181342	CTIAO 2.2 m	FEROS	20	Jones et al. (2016)
HD 181342	Anglo-Australian Telescope	UCLES	5	Wittenmyer et al. (2011)
HD 5608	OAO 1.88 m	HIDES	43	Sato et al. (2012)
HD 10697	Harlan J. Smith Telescop	TCS	32	Wittenmyer et al. (2009)
HD 10697	Hobby–Eberly Telescope	HRS	40	Wittenmyer et al. (2009)
HD 210702	Lick Observatory	Hamilton spectrometer	29	Johnson et al. (2007a)
HD 210702	OAO 1.88 m	HIDES	36	Sato et al. (2012)
HD 214823	Observatoire de Haute-Provence 1.93 m	SOPHIE	13	Díaz et al. (2016)
HD 214823	Observatoire de Haute-Provence 1.93 m	SOPHIE+	11	Díaz et al. (2016)
HD 93396	Lick Observatory (APF)	Levy Spectrometer	15	Pepper et al. (2017)

$R \approx 55{,}000$. For a $V = 8$ magnitude star, the exposure required is 90 s to reach a signal-to-noise ratio of 190 at 5800 Å. RVs are calculated using the iodine-cell calibration technique and the forward-modeling procedure described in Butler et al. (1996) and later Howard et al. (2011). For several stars that were known planet hosts, we included the non-Keck RV measurements as published with the planet discovery. These stars and the instruments used are briefly described below with a summary included in Table 1.

HD 1502—In addition to Keck/HIRES observations HD 1502 was also observed using the Tull Coude Spectrograph (Tull et al. 1995) on the Harlan J. Smith Telescope as well as the High Resolution Spectrograph (Tull 1998) on the Hobby–Eberly Telescope (HET; Ramsey et al. 1998), both of which have $R = 60{,}000$. Differential RVs were computed using the *Austral* I_2-data modeling algorithm (Endl et al. 2000). The velocities are given in Table 2 of Johnson et al. (2011).

HD 159868—HD 159868 was observed mainly with the Anglo-Australian Telescope (AAT) (Jones et al. 2002) using the UCLES echelle spectrograph. RVs are given in Table 2 of Wittenmyer et al. (2012).

HD 192699—HD 192699 was also observed with Lick Observatory's Shane 3 m and 0.6 m Coude Auxiliary Telescopes, which feed into the Hamilton spectrometer (Vogt 1987). The velocities for this star are given in Table 3 of Johnson et al. (2007b).

HD 114613—HD 114613 is another star that was observed as part of the Anglo-Australian Planet Search and has RV measurements from the UCLES echelle spectrograph (Diego et al. 1990). The RVs are given in Table 1 of Wittenmyer et al. (2014).

HD 38801—Additional RV observations of HD 38801 come from the high dispersion spectrograph on the 8.2 m Subaru Telescope (Noguchi et al. 2002). The RV measurements can be found in Table 2 of Harakawa et al. (2010).

HD 181342—HD 181342 (also called HIP 95124) has a number of observations from various instruments, including two telescopes at the Cerro Tololo Inter-American Observatory: the 1.5 m telescope using the CHIRON spectrograph (Tokovinin et al. 2013) and the 2.2 m telescope using the FEROS spectrograph (Kaufer et al. 1999). In addition, it was observed as part of the Pan Pacific Planet Search (Wittenmyer et al. 2011) using the UCLES spectrograph (Diego et al. 1990). All velocities from these instruments are listed in Table A.4 of Jones et al. (2016).

HD 5608—HD 5608 was observed as part of the Okayama Planet Search Program (Sato 2005), which uses the HIgh Dispersion Echelle Spectrograph (HIDES) on the 1.88 m telescope at Okayama Astrophysical Observatory (OAO). The velocities are given in Table 2 of Sato et al. (2012).

HD 10697—HD 10697 was also observed using the two telescopes at McDonald observatory: HET and the 2.7 m Harlan J. Smith telescope. The velocities are given in the electronic version of Table 10 in Wittenmyer et al. (2009).

HD 210702—HD 210702 has observations from both Lick Observatory and OAO. The velocities from Lick are given in Johnson et al. (2007a). The velocities from OAO are given in Table 8 of Sato et al. (2012).

HD 214823—HD 214823 was observed using ELODIE and SOPHIE/SOPHIE+ instruments on the 1.93 m telescope at Observatoire de Haute-Provence. Given ELODIE's large instrumental uncertainty (15–30 m s^{-1}) and that there are only five measurements from ELODIE we use only the RVs from SOPHIE and upgraded SOPHIE+ instruments. This accounts for an additional 24 observations for this star. These velocities are given in Díaz et al. (2016).

HD 93396—HD 93396 (KELT-11) was observed using the Levy spectrograph on the Automated Planet Finder (APF) telescope at Lick Observatory. The velocities are are given in Table 6 of Pepper et. al (2017).

3. Seven New Planets around Subgiants

Here we present the new planets discovered around subgiant stars. All RV time series for every star used in this work are given in Table 4. We note that our quoted values of χ^2 from the fitting procedure RVLIN throughout this paper are significantly larger than 1. The reason is because we have use only the reported internal measurement errors in our fits. Previous works have inflated individual measurement errors by including a "jitter" term in quadrature to account for increased RV variations due to intrinsic stellar variability (Wright 2005). However, given the large known uncertainty in jitter estimates in Wright (2005), we do not follow this approach. Finally, all stellar parameters quoted

here come from B17 and were used to obtain planet parameters where necessary (planet mass, transit probabilities, etc.).

The majority of planets described below have periods >300 days. At these periods, the greatest concern for the planet validity is stellar activity cycles that operate on similar timescales. To avoid misidentifying a stellar activity cycle as a planet, we have examined the simultaneous s-index time series for each of these planets. Except for HD 180053, none of the new planet hosts in this work (including planet candidates in Section 4) show significant activity cycles that correlate with the RVs. Furthermore, none of the stars show evidence of noncycling activity that correlates with the RV measurements. Thus, we are confident that we have identified planet signals rather than activity-induced RVs.

Another timescale of importance is the stellar rotation timescale, which can be hundreds of days for giant stars. For the subgiants in this work we expect that the rotation periods are all much less than the planet periods given that most planet periods here are >300 days. While it is possible that some of the planet periods are on timescales similar to the rotation timescales, the coherence and amplitudes of these signals make it unlikely that they are due to rotationally modulated inhomogeneities.

Lastly, we have examined the spectral window functions of the RV time series as described in Dawson & Fabrycky (2010) to be certain that none of the planets in this work are a result of sparsely sampled data that could introduce spurious periodicity that lead to false peaks in the periodogram. We find that none of the planets in this work correspond to significant peaks in the spectral window function.

We have ordered the new planets in this paper in descending order of detection security, with the most secure detections first. In general we based our threshold for planet status as meeting three main criteria. First, we need to have observed a full period such that $N_p > 1$, where N_p is the number of periods observed, found by simply dividing the baseline of the time series by the best-fit period. We generally wish $N_p \gg 1$ to be certain about a planet but our threshold of 1 makes it necessary to have observed two instances where the velocities have turned over. Second, we examine the false alarm probability (FAP) and choose a 1% FAP threshold. Third, and most important, is the ratio of the semiamplitude to the rms, K/σ. This ratio alone indicates the ability to detect the planet in a single measurement. We expect then that our ability to detect a planet scales with the number of observations and define a detection threshold D

$$D \equiv \frac{K}{\sigma}\sqrt{N - M}, \qquad (1)$$

where N is the number of observations and M is the number of free parameters in the planet fit (six for a one-planet fit plus five for each additional planet and one additional free parameter if the fit includes a linear trend). For a "10σ detection," D must be greater than 10.[11]

3.1. A 1.7 M_{Jup} Planet around HD 72490

HD 72490 is a G5 subgiant with $V = 7.83$, $B - V = 0.95$ and a parallax-based distance of 124.22 pc (Wenger et al. 2000).

It has a radius of ∼5 $R_\odot$, an effective temperature $T_{eff} = 4934$ K, and surface gravity $\log g = 3.210$. A summary of its stellar parameters can be found in Table 2.

The initial observations of this star began in late 2007 and finished in 2014, with only two observations since 2014. It was identified in Butler et al. (2017) as having a planet candidate. The best-fit Keplerian orbital solution yields an orbital period of $P = 858 \pm 12$ days (2.35 yr), velocity semiamplitude $K = 33.5 \pm 1.5$ m s^{-1}, and eccentricity $e = 0.124 \pm 0.046$. From the stellar mass $M_\star = 1.21\ M_\odot$ we derive the minimum mass of the planet $m_p \sin i = 1.768 \pm 0.080\ M_{Jup}$ and semi-major axis $a = 1.88 \pm 0.17$ au. The full set of orbital parameters and corresponding uncertainties are given in Table 3. The time series showing the signal of HD 72490 b is shown in the left panel of Figure 2. A search for a possible second planet yielded nothing of significance, which is supported by the periodogram of the raw RV data along with the periodogram of the data with the best-fit model of HD 72490 b subtracted out (shown in the right panel of Figure 2). For HD 72490 b, the preliminary next predicted transit is BJD 2459074.350 ± 41.296 (2020 December 8). Its most recent predicted transit was in early April of 2018 and before that in late November of 2015, missing its $K2$ Campaign 5 observations by a mere 4 months.

3.2. A Jupiter-mass Planet around HD 94834

HD 94834 is a K1 subgiant with $V = 7.61$, $B - V = 0.99$ (Wenger et al. 2000). It has effective temperature $T_{eff} = 4798$ K, and surface gravity $\log g = 3.22$. A summary of its stellar parameters can be found in Table 2.

Observations of this star span roughly 8.5 yr with the majority of observations between 2010 and 2012. The final five observations demonstrate the periodicity of the signal. HD 94834 was identified in Butler et al. (2017) as having a planet candidate. Our best-fit orbital solution shows a period of 1576 ± 76 days (∼4.3 yr), velocity semiamplitude $K = 20.7 \pm 2.9$ m s^{-1}, and eccentricity $e = 0.14 \pm 0.10$. The minimum mass of this planet is $m_p \sin i = 1.192 \pm 0.017\ M_{Jup}$ with a semimajor axis $a = 2.74 \pm 0.19$ au. The full set of orbital parameters are given in Table 3. Figure 3 shows the time series of HD 94834 b, with the initial and final periodogram for this system.

3.3. A Jupiter Orbiting HD 14787

HD 14787 is a G5 subgiant star with $V = 7.63$ and $B - V = 0.93$ (Wenger et al. 2000). It has a mass of $M_\star = 1.43\ M_\odot$, surface gravity $\log g = 3.23$, and $T_{eff} = 4946$ K. A summary of its stellar parameters can be found in Table 2. Observations of this star span about 9 yr starting in 2007. The best-fit Keplerian solution yields an orbital period of 676.6 ± 8.1 days, velocity semiamplitude 20.7 ± 1.3 m s^{-1}, and eccentricity 0.155. It is only slightly more massive than Jupiter-mass with a minimum mass of $1.121 \pm 0.069\ M_{Jup}$. The full set of orbital parameters can be found in Table 3. We show in Figure 4 the time series for HD 14787 b as well as the periodogram before and after subtracting out HD 14787 b.

3.4. A Jupiter Orbiting HD 13167

HD 13167 is a G3 subgiant star with $V = 8.34$ and $B - V = 0.65$ (Wenger et al. 2000). It has a mass of $M_\star = 1.35\ M_\odot$, surface gravity $\log g = 3.72$, and $T_{eff} = 5671$ K. A summary of

---

[11] We find that these thresholds combine such that a single threshold of $D > 17$ is able to distinguish planet versus candidate. Although arbitrary, this singular threshold is able to match our intuition.

Table 2
Stellar Parameters for Subgiants with Known Companions

Star	R.A. (deg)	Decl. (deg)	V (mag)	Mass ($M_\odot$)	Radius ($R_\odot$)	$T_{\rm eff}$ (K)	$\log g$	$\log R'_{\rm HK}$	$S_{\rm HK}$	$\sigma_{\rm RV}$ (m s^{-1})
(1)	(2)	(3)	(4)	(5)	(6)	(7)	(8)	(9)	(10)	(11)
HD 10697	26.23260	20.08315	6.27	1.13	1.79	5600	3.96	−5.04	0.16	7.856
HD 38529	86.64547	1.16819	5.95	1.41	2.56	5541	3.77	−5.03	0.16	9.531
HD 114613	198.01328	−37.80302	4.85	1.27	2.14	5641	3.87	−5.08	0.15	5.675
HD 117176	202.10753	13.77879	4.97	1.09	1.89	5495	3.95	−5.12	0.14	3.974
HD 159868	264.74802	−43.14551	7.24	1.19	2.13	5534	3.92	−5.02	0.16	5.485
HD 175541	283.92035	4.26533	8.02	1.39	4.19	5013	3.33	−5.18	0.14	6.516
HD 190228	300.75323	28.30686	7.30	1.14	2.51	5238	3.72	−4.98	0.17	4.314
HD 1502	4.82111	14.05475	8.36	1.46	4.67	4947	3.18	−5.15	0.14	11.328
HD 3404	9.19505	−24.50094	7.94	1.17	2.05	5339	3.81	−5.05	0.16	2.120
HD 4313	11.41816	7.84502	7.83	1.63	5.14	4943	3.24	−5.28	0.12	4.695
HD 5319	13.75583	0.78956	8.05	1.27	4.06	4871	3.26	−5.28	0.12	6.802
HD 5608	14.55925	33.95089	5.99	1.53	5.14	4877	3.19	−5.39	0.10	8.206
HD 6019	15.41506	7.30529	7.75	1.12	4.98	5020	3.08	−5.07	0.16	4.390
HD 8375	20.90615	34.24589	6.28	1.62	3.75	5207	3.66	−4.94	0.19	7.937
HD 10011	24.35865	−15.99768	7.99	1.50	4.32	5025	3.28	−5.13	0.14	4.961
HD 10212	25.20706	45.01896	8.13	1.18	4.34	4907	3.14	−5.21	0.14	28.302
HD 10442	25.47143	2.70438	7.84	1.01	1.97	4912	3.19	−5.18	0.14	5.610
HD 11970	29.60127	40.91367	8.23	1.24	3.74	5084	3.44	−5.10	0.15	8.935
HD 13167	32.05743	−24.69541	8.34	1.35	2.39	5671	3.72	−5.12	0.14	3.985
HD 14787	35.80856	10.83675	7.63	1.43	5.01	4946	3.23	−5.18	0.14	5.309
HD 18015	43.36336	−8.84802	7.89	1.49	3.13	5603	3.64	−4.94	0.17	8.407
HD 18667	45.03415	0.23543	8.34	1.05	3.95	4855	3.08	−5.22	0.13	5.167
HD 18742	45.04440	−20.80261	7.81	1.36	5.13	4940	3.09	−5.22	0.13	5.833
HD 21340	51.40204	−27.27249	7.40	1.55	6.32	4908	3.07	−5.22	0.13	5.678
HD 28678	67.85606	4.57530	8.38	1.53	6.48	4972	3.06	−5.27	0.13	5.780
HD 30856	72.57442	−24.36884	7.91	1.17	4.40	4895	3.20	−5.23	0.13	5.518
HD 33142	76.89809	−13.98648	7.96	1.41	4.45	4978	3.40	−5.18	0.14	5.165
HD 38801	86.99657	−8.32770	8.26	1.29	2.41	5207	3.77	−5.02	0.17	14.413
HD 45410	97.69628	58.16263	5.86	1.44	5.20	4938	3.19	−5.29	0.12	3.501
HD 51272	104.59510	37.98798	7.78	1.73	7.00	4870	3.08	−5.19	0.15	23.076
HD 72490	128.40271	13.55079	7.82	1.21	4.96	4934	3.21	−5.19	0.14	6.177
HD 73534	129.81584	12.96037	8.23	1.16	2.58	4917	3.60	−5.24	0.13	4.176
HD 75784	133.09976	13.23344	7.84	1.26	3.40	4867	3.46	−5.24	0.13	4.603
HD 88133	152.53198	18.18687	8.01	1.26	2.20	5392	3.88	−5.18	0.14	4.376
HD 93396	161.70726	−9.39902	8.04	1.46	2.83	5326	3.74	−4.90	0.20	6.886
HD 94834	164.31297	24.14278	7.60	1.11	4.20	4798	3.22	−5.22	0.14	6.319
HD 95089	164.69890	1.72922	7.92	1.54	5.08	4918	3.24	−5.21	0.13	6.798
HD 96063	166.18523	−2.51322	8.21	1.37	4.75	5020	3.33	−5.12	0.15	5.197
HD 96167	166.31279	−10.29130	8.09	1.27	1.94	5733	3.99	−5.16	0.14	4.298
HD 97601	168.63914	52.94690	7.46	1.64	4.66	5062	3.34	−4.67	0.33	20.386
HD 98219	169.44814	−23.97542	8.05	1.41	4.60	4925	3.36	−5.21	0.14	5.914
HD 99706	172.12589	43.96658	7.65	1.46	5.52	4862	3.09	−5.25	0.13	11.989
HD 102956	177.84380	57.64074	7.86	1.66	4.55	4985	3.38	−5.07	0.18	6.300
HD 106270	183.40535	−9.51338	7.58	1.39	2.66	5509	3.72	−4.90	0.19	10.294
HD 108863	187.58296	21.94824	7.71	1.59	5.74	4878	3.07	−5.27	0.13	6.186
HD 112988	195.04286	34.99842	7.76	1.04	5.25	4852	3.25	−5.21	0.13	8.404
HD 125390	214.53883	38.96698	8.21	1.36	6.47	4850	3.13	−5.21	0.14	8.013
HD 125607	214.86337	37.60997	8.09	1.47	4.31	4985	3.34	−5.16	0.14	17.358
HD 131496	223.34595	18.23540	7.80	1.34	4.44	4846	3.18	−5.33	0.12	7.183
HD 238433	228.40825	57.19163	8.37	1.37	5.09	4936	3.13	−5.14	0.15	9.793
HD 142091	237.80804	35.65738	4.79	1.50	4.85	4871	3.26	−5.31	0.12	2.838
HD 145428	242.96356	−25.88357	7.73	1.02	5.70	4779	3.13	−5.29	0.13	4.440
HD 148284	246.45174	30.26513	9.01	1.07	1.48	5572	3.97	−5.14	0.14	3.085
HD 152581	253.43159	11.97375	8.38	1.30	5.14	5027	3.29	−5.14	0.15	4.730
HD 163607	268.41873	56.39196	8.00	1.12	1.76	5522	3.97	−5.01	0.16	2.878
HD 180053	288.40088	34.91454	7.93	1.75	4.06	5131	3.54	−4.73	0.31	13.381
HD 180902	289.82319	−23.55816	7.78	1.41	4.16	4961	3.36	−5.13	0.15	1.944
HD 181342	290.26764	−23.61957	7.55	1.69	4.71	4945	3.28	−5.31	0.12	10.681
HD 185269	294.29892	28.49986	6.67	1.30	2.00	5923	3.92	−5.03	0.15	7.018
HD 192699	304.02502	4.58079	6.44	1.38	4.41	5041	3.25	−5.26	0.12	8.623
HD 193342	304.25226	56.90459	8.07	1.69	6.01	4913	3.19	−5.21	0.14	7.438
HD 195787	307.64395	58.28724	7.63	1.40	4.87	4961	3.26	−5.16	0.14	3.395

Table 2
(Continued)

Star	R.A. (deg)	Decl. (deg)	V (mag)	Mass ($M_\odot$)	Radius ($R_\odot$)	$T_{\rm eff}$ (K)	$\log g$	$\log R'_{\rm HK}$	$S_{\rm HK}$	$\sigma_{\rm RV}$ (m s^{-1})
(1)	(2)	(3)	(4)	(5)	(6)	(7)	(8)	(9)	(10)	(11)
HD 196645	309.58716	13.33141	7.80	1.28	3.39	5041	3.43	−5.14	0.15	4.700
HD 200964	316.66602	3.80312	6.48	1.39	4.92	4982	3.22	−5.12	0.15	4.996
HD 206610	325.85376	−7.40825	8.34	1.55	6.12	4842	3.22	−5.25	0.14	4.544
HD 207077	326.68353	−8.00718	8.24	1.13	3.95	5067	3.27	−5.08	0.15	6.690
HD 210702	332.96387	16.04055	5.93	1.61	4.92	4951	3.28	−5.26	0.12	6.394
HD 212771	336.76279	−17.26365	7.60	1.56	5.27	5003	3.31	−5.14	0.14	7.794
HD 214823	340.08279	31.78759	8.06	1.31	2.04	5933	3.92	−5.08	0.15	12.641
HD 4917	12.77615	−12.92760	8.03	1.32	5.01	4802	2.97	−5.33	0.12	5.374

Note. Host star parameters for all planets listed in Table 5. Column 1 lists the star name. Columns 2 and 3 give the coordinates. Data in columns 4–10 come from Brewer et al. (2016). Column 4 gives the V-band magnitude. Columns 5, 6, and 7 list the mass, radius, and effective temperature of the star. Column 8 gives the spectroscopic surface gravity. Columns 9 and 10 give two measures of chromospheric activity. We note that for most subgiants in this sample, the $\log R'_{\rm HK}$ value is not calibrated, which is why we have also included $S_{\rm HK}$. Finally, column 11 gives the measured RV rms after subtracting the planetary signal.

(This table is available in machine-readable form.)

its stellar parameters can be found in Table 2. Observations of this star span about 8 yr starting in late 2007. The best-fit Keplerian solution yields an orbital period of 2613 ± 17 days, and velocity semiamplitude 48.2 ± 2.7 m s^{-1} on a fairly eccentric orbit ($e = 0.563 \pm 0.033$). It has a minimum mass of 3.31 ± 0.16 $M_{\rm Jup}$. The full set of orbital parameters can be found in Table 3. We show in Figure 5 the time series for HD 13167 b as well as the periodogram before and after subtracting out HD 13167 b. The final observation in the time series (Figure 5) is what secures this detection, as we have now observed it reaching a second maximum.

3.5. A Jupiter Orbiting HD 18015

HD 18015 is a G6 subgiant star with $V = 7.89$ and $B − V = 0.68$ (Wenger et al. 2000). It has a mass of $M_\star = 1.49\ M_\odot$, surface gravity $\log g = 3.64$, and $T_{\rm eff} = 5603$ K. A summary of its stellar parameters can be found in Table 2. Observations of this star span about 8 yr starting in late 2007. The best-fit Keplerian solution yields an orbital period of 2278 ± 71 days, and velocity semiamplitude 38.0 ± 2.7 m s^{-1}, and eccentricity 0.148 ± 0.061. It has a minimum mass of 3.18 ± 0.23 $M_{\rm Jup}$. The full set of orbital parameters can be found in Table 3. We show in Figure 6 the time series of HD 18015 b as well as the periodogram before and after subtracting out HD 18015 b.

3.6. A Jupiter Orbiting HD 180053

HD 180053 is a K0 subgiant star with $V = 7.93$ and $B − V = 0.92$ (Wenger et al. 2000). It has a mass of $M_\star = 1.75\ M_\odot$, surface gravity $\log g = 3.54$, and $T_{\rm eff} = 5131$ K. A summary of its stellar parameters can be found in Table 2. Observations of this star span about 8 yr starting in 2007. HD 180053 was identified in Butler et al. (2017) as having a planet candidate. The best-fit Keplerian solution yields an orbital period of 213.72 ± 0.47 days, and velocity semiamplitude 51.5 ± 1.4 m s^{-1}, and eccentricity 0.081 ± 0.029. It has a minimum mass of 2.194 ± 0.063 $M_{\rm Jup}$. The full set of orbital parameters can be found in Table 3. We show in Figure 7 the time series for HD 180053 b as well as the periodogram before and after subtracting out HD 180053 b. We also include in Figure 8 the phase-folded RV curve to help show the planet

signal more clearly. We note that both the phase curve and final periodogram show evidence of additional RV variations beyond simply one planet. Once we remove the best single-planet fit, we find a correlation between the RVs and the chromospheric activity as measured by the Ca II H and K lines using the Mount Wilson s-index, $S_{\rm HK}$, measured following the same procedure as in Isaacson & Fischer (2010). Given that we obtain poor two- and three-planet fits, we expect that the additional RV variations are simply activity-induced, with timescales near 70 and 600 days, reasonable timescales for modulation from stellar rotation and stellar activity cycles.

3.7. A Jupiter Orbiting HD 4917

HD 4917 is a K0 subgiant (Wenger et al. 2000). It has a temperature of $T_{\rm eff} = 4802$ K and mass 1.32 $M_\odot$. Additional stellar properties can be found in Table 2. There are nearly 50 observations of this star that span close to 10 yr. Here we present the discovery of a $m_{\rm p} \sin i = 1.615 \pm 0.093\ M_{\rm Jup}$ planet on a 400.5 ± 1.7 day orbit and its phase curve is shown in the left panel of Figure 9. The right panel shows the periodogram before and after subtracting out the best-fit planet.

We note that the final periodogram of the residual shows two intriguing signals: one near 800 days and one near 1000 days. Our best three-planet fit provided the best overall fit; however, we decline to call the outer two real planets for now because we have not done the requisite dynamical analysis to show that the orbits we derive for them are stable. Instead, we consider the outer two signals as planet candidates, which are discussed in Section 4.

4. Eight Candidate Planetary Signals around Subgiant Stars

The following signals are likely due to planetary companions. They are intriguing and likely correct; however, they do not rise to the level of the others by not meeting one or more of our detection thresholds, as described in Section 3. We include them here for the purposes of listing possible transit parameters and as long-period planets, as it is uncertain whether more data is forthcoming. We encourage continued observations of these systems to fully confirm these planets. The reason for each planet candidate's status as a candidate is listed individually.

Table 3
Orbital Parameters

Star	Com	$m \sin i$ $(M_{\rm Jup})$	R $(R_{\rm Jup})$	P (days)	a	$T_{\rm p}$ (JD-2440,000)	e	ω (degrees)	K (m s^{-1})	γ (m s^{-1})	$dvdt$	Orbit Ref
(1)	(2)	(3)	(4)	(5)	(6)	(7)	(8)	(9)	(10)	(11)	(12)	(13)
HD 10697	b	6.383(80)	1.152	1075.69(82)	2.140(95)	11492(17)	0.1043(83)	114.9(6.0)	116.9(1.3)	−9.15(82)	0	Wittenmyer et al. (2009)
HD 38529	b	0.797(15)	1.268	14.30944(30)	0.1294(58)	14384.59(16)	0.280(17)	89.8(4.4)	55.2(1.1)	8.83(74)	0	Wright et al. (2009)
⋯	c	12.99(15)	1.123	2136.1(3.1)	3.64(16)	12255.9(8.1)	0.3407(69)	18.4(1.4)	172.4(1.3)	0.0(0.0)	0	Wright et al. (2009)
HD 114613	b	0.357(32)	1.182	4000(120)	5.34(26)	15150(90)	0.458(89)	196(11)	4.38(40)	2.62(65)	0	Wittenmyer et al. (2014)
HD 117176	b	7.416(54)	1.142	116.6880(54)	0.481(21)	15291.721(86)	0.3988(19)	359.83(29)	316.20(78)	−51.25(53)	0	Butler et al. (2006)
HD 159868	b	2.218(59)	1.202	1184.1(7.1)	2.32(12)	13670(190)	0.024(19)	63(76)	37.92(97)	−6.42(92)	0	Wittenmyer et al. (2012)
⋯	c	0.768(44)	1.269	351.0(1.1)	1.032(55)	13225(13)	0.184(37)	272(16)	20.0(1.1)	0.0(0.0)	0	Wittenmyer et al. (2012)
HD 175541	b	0.598(29)	1.277	298.43(45)	0.975(89)	10155(25)	0.110(49)	129(28)	14.68(71)	2.06(56)	0	Johnson et al. (2007a)
HD 190228	b	4.300(59)	1.166	1143.5(1.6)	2.24(12)	13521.1(3.5)	0.5571(99)	94.6(1.5)	92.0(1.1)	12.39(77)	0	Wittenmyer et al. (2009)
HD 1502	b	2.75(16)	1.183	428.5(1.2)	1.26(12)	15170(67)	0.031(22)	126(58)	57.5(3.3)	1.32(94)	0	Johnson et al. (2011)
HD 3404	*	152.0(6.4)	1.727	1543.54(60)	2.75(17)	13438.3(4.9)	0.7440(59)	0.37(21)	3332(17)	116(26)	0	Binary
HD 4313	b	1.927(90)	1.212	356.21(88)	1.157(95)	14816(12)	0.147(47)	102(13)	40.3(1.7)	−13.6(1.7)	0	Johnson et al. (2010a)
HD 5319	b	1.556(42)	1.227	637.1(1.4)	1.57(12)	16382(26)	0.092(25)	158(15)	31.46(83)	−7.21(98)	0.00253(59)	Robinson et al. (2007)
⋯	c	1.053(72)	1.254	872.2(6.0)	1.93(15)	13443(58)	0.183(64)	244(25)	19.4(1.4)	0.0(0.0)	0	Giguere et al. (2015)
HD 5608	b	1.681(81)	1.222	779.5(4.9)	1.911(92)	12420(110)	0.056(39)	294(54)	28.0(1.4)	39.5(2.8)	−0.0165(12)	Sato et al. (2012)
HD 6019	*	409(36)	4.132	2457.00(19)	3.70(32)	21712.74(70)	0.8170(44)	31.18(49)	8120(240)	786(13)	0	Binary
HD 8375	*	154.3(4.1)	1.751	83.9664(90)	0.441(21)	16221.11(91)	0.0127(10)	319.0(3.9)	4898.7(4.1)	−1506(48)	0.484(21)	Binary
HD 10011	*	609(54)	5.884	1518.3(1.2)	2.96(26)	14807.90(59)	0.30677(91)	87.95(19)	6941.7(2.0)	1816.7(1.7)	0	Binary
HD 10212	*	664(67)	6.353	3353(16)	4.63(41)	15782.5(2.1)	0.5040(30)	104.29(29)	7021.3(9.7)	−1873(12)	0	Binary
HD 10442	b	1.487(82)	1.230	1032.3(8.9)	2.01(54)	17226(69)	0.132(44)	262(25)	29.9(1.6)	−8.0(1.1)	0	Giguere et al. (2015)
HD 11970	*	577(58)	5.611	8500(140)	8.76(85)	15241.7(1.3)	0.6131(43)	245.56(19)	4933.8(4.2)	1014(12)	0	Binary
HD 13167	b	3.31(16)	1.167	2613(17)	4.10(43)	22162(54)	0.563(33)	265(6.0)	48.2(2.7)	−10.4(1.2)	0	This Work
HD 14787	b	1.121(69)	1.250	676.6(8.1)	1.70(17)	15555(49)	0.155(73)	343(28)	20.7(1.3)	−1.7(1.1)	0	This Work
HD 18015	b	3.18(23)	1.170	2278(71)	3.87(31)	14730(170)	0.148(61)	265(29)	38.0(2.7)	−5.5(1.8)	0	This Work
HD 18667	*	309(38)	3.221	4376(13)	5.32(73)	15016.83(30)	0.66577(78)	288.968(85)	4218.0(2.2)	−312.6(3.7)	0	Binary
HD 18742	b	3.4(1.2)	1.166	766(25)	1.82(16)	15280(140)	0.040(35)	190(74)	61(22)	−2.4(3.7)	0.0026(19)	Johnson et al. (2011)
⋯	c	2.4(1.2)	1.194	859(41)	1.96(17)	1910(670)	0.056(52)	203(63)	42(22)	0.0(0.0)	0	This Work
HD 21340	*	135.9(6.0)	1.566	1249.7(2.5)	2.63(20)	15227.4(1.3)	0.5612(90)	129.29(85)	2193(51)	53.4(8.8)	0	Binary
HD 28678	b	1.542(73)	1.228	380.2(1.6)	1.18(18)	15513(18)	0.149(47)	128(19)	32.9(1.4)	−23.5(3.4)	0.0124(19)	Johnson et al. (2011)
HD 30856	b	1.547(91)	1.228	847(20)	1.85(13)	15200(150)	0.061(58)	171(68)	29.9(1.7)	5.4(1.7)	0	Johnson et al. (2011)
HD 33142	b	1.385(64)	1.239	326.0(1.2)	1.070(90)	15329(42)	0.066(41)	146(49)	30.7(1.4)	−8.0(1.1)	0	Johnson et al. (2011)
⋯	c	0.62(11)	1.277	809(26)	1.96(17)	−150(500)	0.16(15)	126(60)	10.3(1.8)	0.0(0.0)	0	This Work
HD 38801	b	10.13(24)	1.134	686.8(1.4)	1.66(11)	13849(27)	0.059(26)	296(14)	196.3(3.8)	−26.4(2.7)	0	Harakawa et al. (2010)
HD 45410	b	2.010(77)	1.209	934.3(8.6)	2.11(10)	15384(94)	0.073(36)	130(38)	32.8(1.2)	4.4(1.1)	0	Bowler et al. (2010)
HD 51272	*	839(97)	7.815	5660(680)	7.5(1.2)	15871.5(1.8)	0.669(22)	202.56(61)	6930(130)	3540(360)	0	Binary
HD 72490	b	1.768(80)	1.218	858(12)	1.88(17)	320(230)	0.124(46)	145(23)	33.5(1.5)	−3.4(3.3)	0.0026(20)	This Work
HD 73534	b	1.112(59)	1.251	1750(24)	2.99(18)	17100(130)	0.126(57)	168(23)	17.11(93)	−1.67(68)	0	Valenti et al. (2009)
HD 75784	b	1.00(14)	1.258	341.2(1.1)	1.032(68)	41(67)	0.097(63)	350(200)	24.9(3.5)	−30.5(9.5)	0	Giguere et al. (2015)
⋯	c	5.64(72)	1.161	7900(2000)	8.4(1.4)	−8800(5900)	0.489(92)	325(12)	56.5(5.2)	0.0(0.0)	0	Giguere et al. (2015)
HD 88133	b	0.2845(63)	1.045	3.414884(30)	0.0479(32)	13016.82(37)	0.031(21)	43(33)	32.93(73)	2.07(53)	0	Butler et al. (2006)
HD 93396	b	0.201(16)	0.857	4.73650(52)	0.0626(50)	17062.26(49)	0.166(91)	115(39)	19.2(1.6)	7.7(4.7)	−0.0019(16)	Pepper et al. (2017)
HD 94834	b	1.26(17)	1.242	1576(76)	2.74(19)	16100(190)	0.14(10)	38(41)	20.7(1.9)	−2.4(1.5)	0	This Work
HD 95089	b	3.45(14)	1.165	1785(32)	3.33(30)	1170(260)	0.284(42)	66(10)	45.1(1.9)	−15.4(1.3)	0	Johnson et al. (2010a)
⋯	c	1.260(85)	1.242	464.4(3.8)	1.36(12)	70(130)	0.119(72)	301(35)	25.0(1.6)	0.0(0.0)	0	Bryan et al. (2016)
HD 96063	b	1.27(27)	1.242	362.5(2.2)	1.11(11)	15165(43)	0.17(11)	271(51)	29.6(6.8)	−14.0(3.9)	0	Johnson et al. (2011)
HD 96167	b	0.717(40)	1.272	498.04(76)	1.332(91)	13061.1(4.4)	0.685(29)	290.1(6.1)	21.5(1.4)	−0.80(53)	0	Peek et al. (2009)
HD 97601	*	367(31)	3.752	4140(390)	5.95(62)	16576(12)	0.3365(68)	50.7(4.9)	3120(69)	−460(210)	0	Binary
HD 98219	b	1.964(99)	1.210	433.8(2.0)	1.258(95)	14633(47)	0.079(40)	360(200)	42.0(2.1)	3.5(1.4)	0	Johnson et al. (2011)
HD 99706	b	1.23(19)	1.244	841(36)	1.98(15)	15310(89)	0.25(16)	50(44)	21.2(3.9)	−5.4(6.7)	0.0016(33)	Johnson et al. (2011)
HD 102956	b	0.960(23)	1.261	6.49470(19)	0.0807(66)	15351.45(64)	0.037(19)	301(33)	74.6(1.8)	−3.0(1.1)	0	Johnson et al. (2010a)
HD 106270	b	10.13(27)	1.134	1888(16)	3.34(21)	16635(37)	0.185(27)	3.3(6.1)	135.4(3.5)	9.8(4.8)	0.0086(27)	Johnson et al. (2011)
HD 108863	b	2.414(78)	1.194	437.7(2.8)	1.32(11)	15558(77)	0.032(27)	191(64)	47.4(1.5)	−5.1(1.5)	0	Johnson et al. (2011)

7

Table 3
(Continued)

Star (1)	Com (2)	$m \sin i$ ($M_{\rm Jup}$) (3)	R ($R_{\rm Jup}$) (4)	P (days) (5)	a (6)	$T_{\rm p}$ (JD-2440,000) (7)	e (8)	ω (degrees) (9)	K (m s^{-1}) (10)	γ (m s^{-1}) (11)	$dvdt$ (12)	Orbit Ref (13)
HD 112988	*	346(28)	3.559	5780(520)	6.38(71)	16299.0(3.6)	0.7246(74)	156.7(3.1)	4610(290)	−818(15)	0	Binary
HD 125390	*	22.16(96)	1.081	1756.2(3.9)	3.16(36)	15914.0(6.7)	0.591(14)	342.4(1.2)	373(16)	−39.8(3.7)	0	Binary
HD 125607	*	379(29)	3.857	578.54(13)	1.55(14)	15495.77(54)	0.4084(24)	17.90(41)	6763(31)	−83(10)	0	Binary
HD 131496	b	1.80(10)	1.217	896(16)	2.01(15)	16114(50)	0.181(60)	58(19)	31.6(1.8)	3.6(1.3)	0	Johnson et al. (2011)
HD 238433	*	748(73)	7.060	1816.89(26)	3.24(28)	14419.92(43)	0.6106(27)	332.02(24)	9644(87)	886(11)	0	Binary
HD 142091	b	1.811(57)	1.216	1285(14)	2.65(12)	16830(51)	0.167(32)	194(14)	26.18(86)	−1.74(60)	0	Baines et al. (2013)
HD 145428	*	343(28)	3.533	5610(350)	6.22(63)	15367.4(5.0)	0.352(25)	309.73(79)	3436(19)	−2129(87)	0	Binary
HD 148284	*	34.50(96)	1.067	339.302(26)	0.974(79)	15786.93(12)	0.38967(97)	35.53(15)	1022.7(1.4)	63.21(82)	0	Binary
HD 152581	b	1.869(68)	1.214	686.5(4.8)	1.66(21)	15040(120)	0.040(31)	181(66)	36.2(1.3)	5.21(97)	0	Johnson et al. (2011)
HD 163607	b	0.7836(98)	1.269	75.2203(94)	0.362(16)	14185.93(15)	0.7441(71)	79.6(1.3)	52.34(74)	54(33)	0	Giguere et al. (2012)
⋯	c	2.201(37)	1.202	1272.0(4.4)	2.39(11)	15111(40)	0.080	274(12)	38.37(65)	0.0(0.0)	0	Giguere et al. (2012)
⋯	d	7.8(3.7)	1.139	37000(13000)	22.4(3.8)	−95000(42000)	0.42(23)	175(92)	49(22)	0.0(0.0)	0	This Work
HD 180053	b	2.194(63)	1.203	213.72(47)	0.843(53)	15197(13)	0.081(29)	76(21)	51.5(1.4)	2.6(1.1)	0	This Work
HD 180902	b	1.685(41)	1.221	510.9(1.5)	1.40(11)	15055(17)	0.107(22)	181(12)	34.25(84)	259(12)	0	Johnson et al. (2010a)
⋯	*	98.7(7.6)	1.186	5880(440)	7.15(66)	1100(1200)	0.335(25)	73.3(1.6)	898(28)	0.0(0.0)	0	Binary
⋯	c	0.099(14)	0.564	15.9058(55)	0.139(11)	−75.7(5.5)	0.28(13)	67(41)	6.6(1.1)	0.0(0.0)	0	This Work
HD 181342	b	2.54(19)	1.190	564.1(4.1)	1.59(10)	21090(220)	0.022(51)	290(110)	44.1(3.3)	−8.4(2.3)	0	Johnson et al. (2010a)
HD 185269	b	1.010(14)	1.257	6.83776(27)	0.0770(37)	13154.25(11)	0.229(14)	176.2(3.5)	93.3(1.4)	−4.06(86)	0	Johnson et al. (2006)
HD 192699	b	2.096(93)	1.206	340.94(92)	1.063(54)	14079(36)	0.082(41)	87(37)	49.3(2.1)	22.9(3.3)	0	Bowler et al. (2010)
HD 193342	*	380(200)	3.881	10000(16000)	10.6(5.6)	15218(82)	0.33(23)	204.5(9.4)	2390(580)	2200(1400)	0	Binary
HD 195787	*	531(40)	5.209	1909.26(37)	3.37(26)	15589.33(70)	0.2692(43)	84.91(48)	5873(28)	3315(12)	0	Binary
HD 196645	b	0.497(44)	1.273	128.94(41)	0.542(35)	15379(17)	0.106(91)	89(46)	17.1(1.6)	2.7(1.1)	0	This Work
HD 200964	b	1.599(67)	1.225	606.3(3.8)	1.565(79)	15350(49)	0.087(35)	133(30)	30.9(1.3)	−6.16(72)	0	Johnson et al. (2011)
⋯	c	1.214(72)	1.244	852.5(7.1)	1.96(10)	15044(29)	0.243(47)	301(13)	21.5(1.3)	0.0(0.0)	0	Johnson et al. (2011)
HD 206610	b	2.036(62)	1.208	673.2(3.3)	1.74(23)	14724(34)	0.100(42)	334(16)	35.4(1.0)	29.8(2.5)	−0.0242(15)	Johnson et al. (2010a)
HD 207077	b	1.16(10)	1.248	606.3(5.6)	1.46(14)	15967(40)	0.204(99)	248(26)	26.2(2.5)	−10.3(1.5)	0	This Work
HD 210702	b	1.808(97)	1.216	354.10(70)	1.148(55)	14042(64)	0.028(34)	189(66)	37.8(2.0)	15.7(1.5)	0	Bowler et al. (2010)
HD 212771	b	2.39(27)	1.195	380.7(1.4)	1.192(99)	14920(52)	0.076(51)	29(65)	50.0(5.8)	14.1(3.3)	0	Johnson et al. (2010a)
HD 214823	*	20.56(32)	1.082	1853.9(1.6)	3.23(20)	15642.1(8.6)	0.1633(36)	122.9(1.7)	285.2(1.3)	−13.48(90)	0	Binary
HD 4917	b	1.615(93)	1.224	400.5(1.7)	1.17(10)	−212(84)	0.066(41)	313(34)	37.1(2.2)	5.7(1.7)	0	This Work
⋯	c	1.37(13)	1.236	821(13)	1.88(17)	1000(230)	0.467(88)	45(11)	27.9(3.7)	0.0(0.0)	0	This Work
⋯	d	0.89(10)	1.264	1093(37)	2.28(21)	450(530)	0.28(14)	296(27)	15.2(2.2)	0.0(0.0)	0	This Work

Note. Orbital parameters and uncertainties for all planets listed in Table 5. Uncertainties are given in parenthetical format, whereby the value has been rounded to the appropriate significant digit, and the listed uncertainty is of the same order (e.g., 1.93 (17) is the same as writing 1.93 ± 0.17)). Columns 1 and 2 list the star and planet designations, as in Table 5. Column 3 lists the minimum mass of the planet. Column 4 gives the estimated radius from FORECAST (Chen & Kipping 2017) used for transit calculations. Column 5 gives the best-fit period. Column 6 gives the calculated semimajor axis of the planet's orbit. Columns 7–12 give the remaining best-fit orbital parameters: time of periastron crossing (column 7), eccentricity (column 8), argument of periastron (column 9), semiamplitude (column 10), the systemic velocity (column 11), and the linear trend parameter (column 12). Finally, column 13 lists the reference used as initial input orbital parameters for the known planets. New orbital companions are listed as "This Work" if they are planetary companions ($m \sin i < 14 \, M_{\rm Jup}$) or "Binary" if their minimum mass indicates they are a brown dwarf or larger mass. We have not performed an extensive search on the previous literature of the binary companions. We have only included those that have well-constrained orbits. This is discussed more in Section 5 and all binary time series are shown in Figure 24.

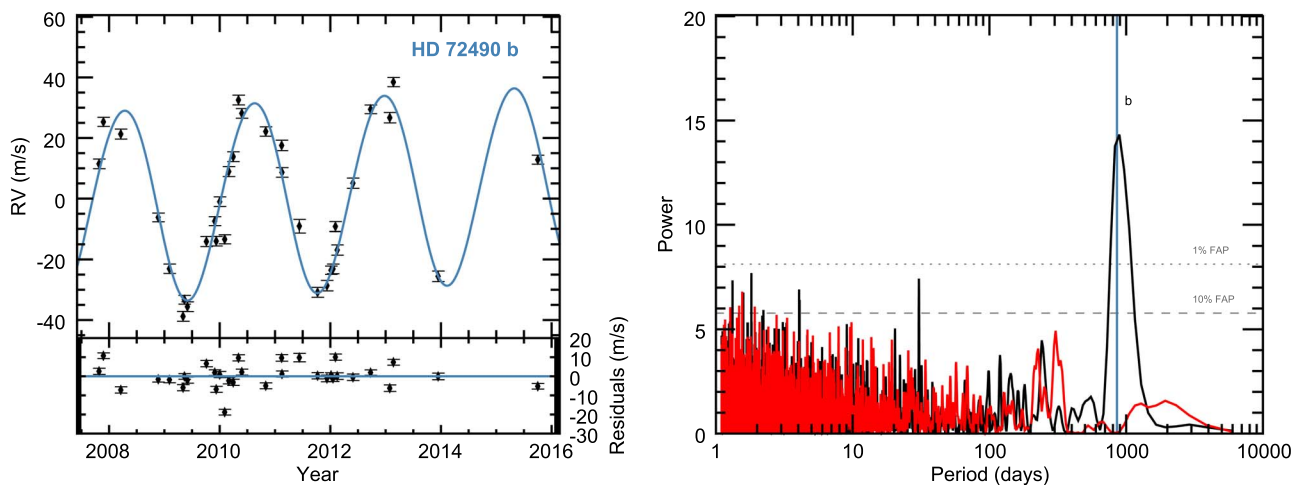(This table is available in machine-readable form.)
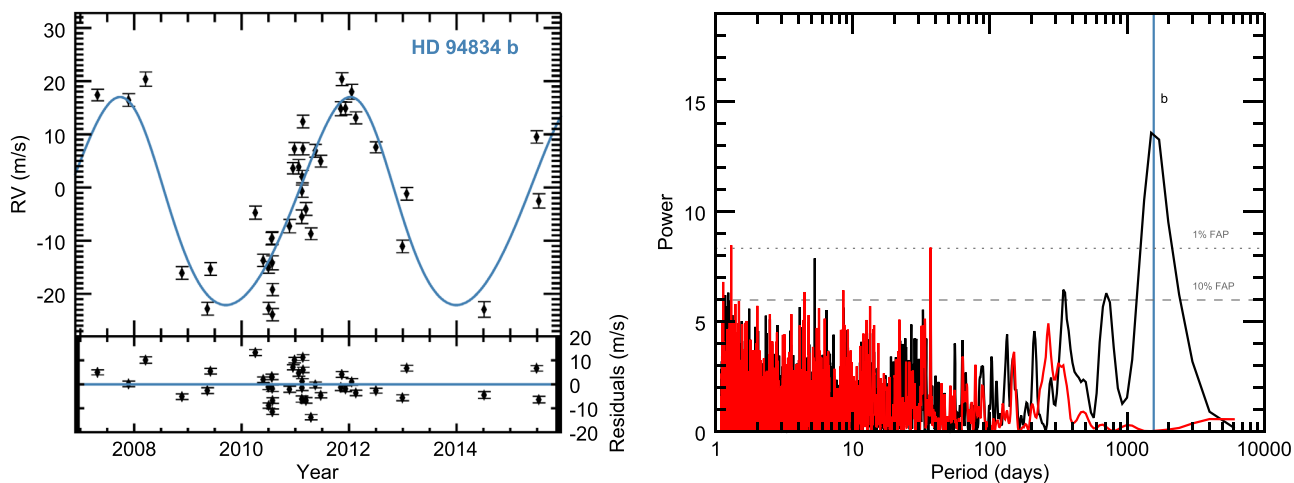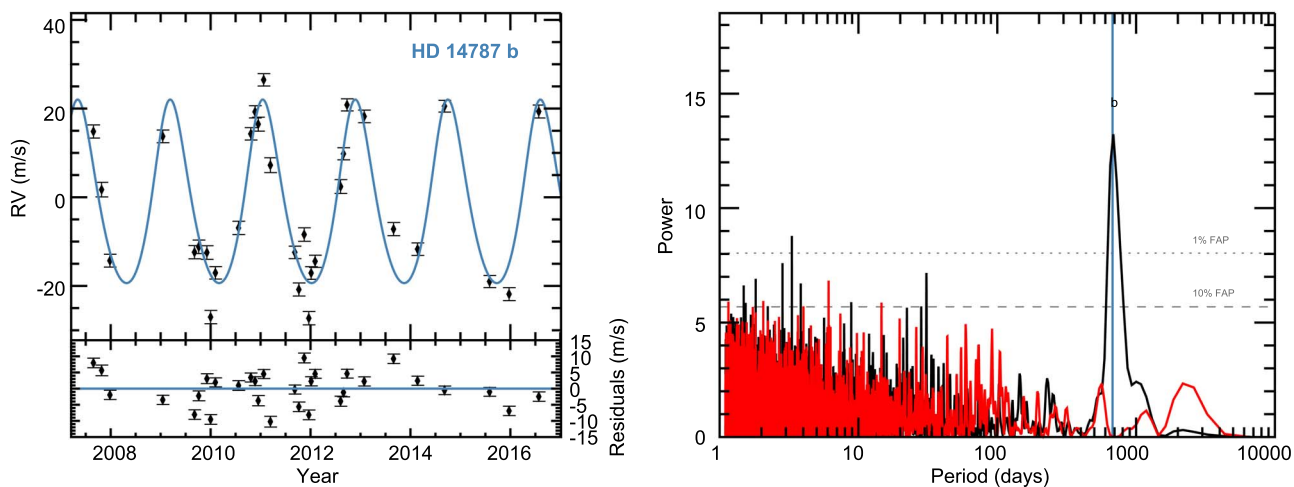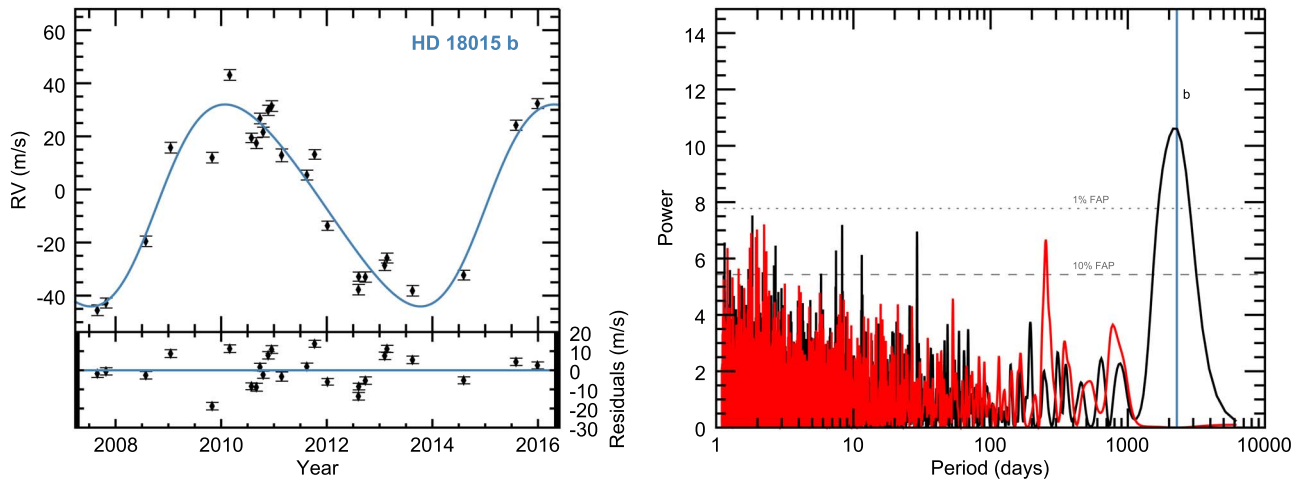
Luhn et al.

Figure 2. (Left) Time series and best-fit orbital solution for HD 72490 b, which has period $P = 858.67$ days, eccentricity $e = 0.0569$, and minimum mass $m_p \sin i = 1.709\ M_{\text{Jup}}$. The residuals are shown in the bottom panel, which have an RV rms $= 6.43$ m s^{-1}. The remaining best-fit parameters can be found in Table 3. (Right) Periodogram of HD 72490 RV data before (black) and after (red) subtracting the best-fit planet parameters for HD 72490 b. The vertical line indicates the best-fit period of HD 72490 b.

Figure 3. (Left) Time series and best-fit orbital solution for HD 94834 b, which has period $P = 1576$ days, eccentricity $e = 0.107$, and minimum mass $m_p \sin i = 1.2$ M_{Jup}. The residuals are shown in the bottom panel, which have an RV rms $= 6.32$ m s^{-1}. The remaining best-fit parameters and uncertainties can be found in Table 3. (Right) Periodogram of HD 94834 RV data before (black) and after (red) subtracting the best-fit planet parameters for HD 94834 b. The vertical line indicates the best-fit period of HD 94834 b.

Figure 4. (Left) Time series and best-fit orbital solution for HD 14787 b, which has period $P = 676$ days, eccentricity $e = 0.155$, and minimum mass $m_p \sin i = 1.12$ M_{Jup}. The residuals are shown in the bottom panel, which have an RV rms $= 5.3$ m s^{-1}. The remaining best-fit parameters can be found in Table 3. (Right) Periodogram of HD 14787 RV data before (black) and after (red) subtracting the best-fit planet parameters for HD 14787 b. The vertical line indicates the best-fit period of HD 14787 b.
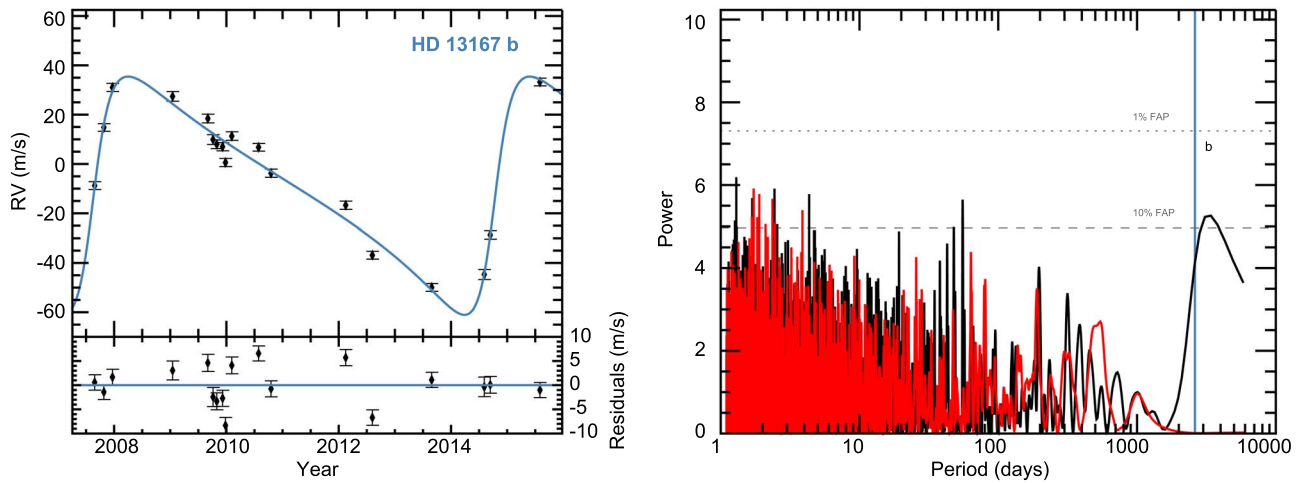
Figure 5. (Left) Time series and best-fit orbital solution for HD 13167 b, with period $P = 2613$ days, eccentricity $e = 0.563$, and minimum mass $m_p \sin i = 3.31$ $M_{\rm Jup}$. The residuals are shown in the bottom panel, which have an RV rms = 4.0 m s^{-1}. The remaining best-fit parameters can be found in Table 3. (Right) Periodogram of HD 13167 RV data before (black) and after (red) subtracting the best-fit planet parameters for HD 13167 b. The vertical line indicates the best-fit period of HD 13167 b. The peak in the periodogram is only barely visible because the time baseline of observations is only slightly longer than 1 period.

Figure 6. (Left) Time series and best-fit orbital solution for HD 18015 b, which has period $P = 2278$ days, eccentricity $e = 0.148$, and minimum mass $m_p \sin i = 3.18$ $M_{\rm Jup}$. The residuals are shown in the bottom panel, which have an RV rms = 8.4 m s^{-1}. The remaining best-fit parameters can be found in Table 3. (Right) Periodogram of HD 18015 RV data before (black) and after (red) subtracting the best-fit planet parameters for HD 18015 b. The vertical line indicates the best-fit period of HD 18015 b.

4.1. Two Possible Additional Planets around HD 4917

The two additional signals around HD 4917, planets c and d, described above are both convincing signals. HD 4917 c has an orbital period $P = 821 \pm 13$ days, eccentricity $e = 0.467 \pm 0.088$, and minimum mass $m_p \sin i = 1.37 \pm 0.13\ M_{\rm Jup}$ and HD 4917 d has orbital period $P = 1093 \pm 37$ days, eccentricity $e = 0.28 \pm 0.14$, and minimum mass $m_p \sin i = 0.89 \pm 0.1$ $M_{\rm Jup}$. The time series for each of these planets can be found in Figure 10 as well as a periodogram before and after subtracting out these two additional signals (HD 4917b was discussed in Section 3). The full time series including the three-planet fit is shown in Figure 11. However, given the proximity of these two additional signals, we feel that this system warrants additional dynamical investigations to ascertain the stability of this planetary system. That detailed investigation is beyond the scope of this work and so we consider these two signals as planetary candidates, despite passing our planet thresholds.

4.2. A Possible Second Planet around HD 18742

HD 18742 is a G8/K0 IV star (Wenger et al. 2000) with one previously known planet (Johnson et al. 2011). It has a V magnitude $V = 7.81$, effective temperature $T_{\rm eff} = 4940$ K, and $\log g = 3.09$. Its mass is 1.36 $M_\odot$ and it has a radius of 5.13 $R_\odot$. Additional stellar properties and uncertainties can be found in Table 2. There are 37 RV observations for this star, all from Keck, which span more than 8 yr (2007 to late 2015). Here we make use of the additional 11 points that span the last 4.5 yr of the 8 yr of observations. The original fit for this planet in Johnson et al. (2011) included a linear trend. Indeed, after refitting this planet and subtracting out the new best fit to HD 18742 b (period $P = 766 \pm 25$ days, eccentricity $e = 0.040 \pm 0.035$, and minimum mass $m_p \sin i = 3.4 \pm 1.2\ M_{\rm Jup}$), there was a substantial peak in the periodogram near 900 days, shown in Figure 12. Refitting the RVs with a two-planet fit starting with a second planet near 900 days resulted in an
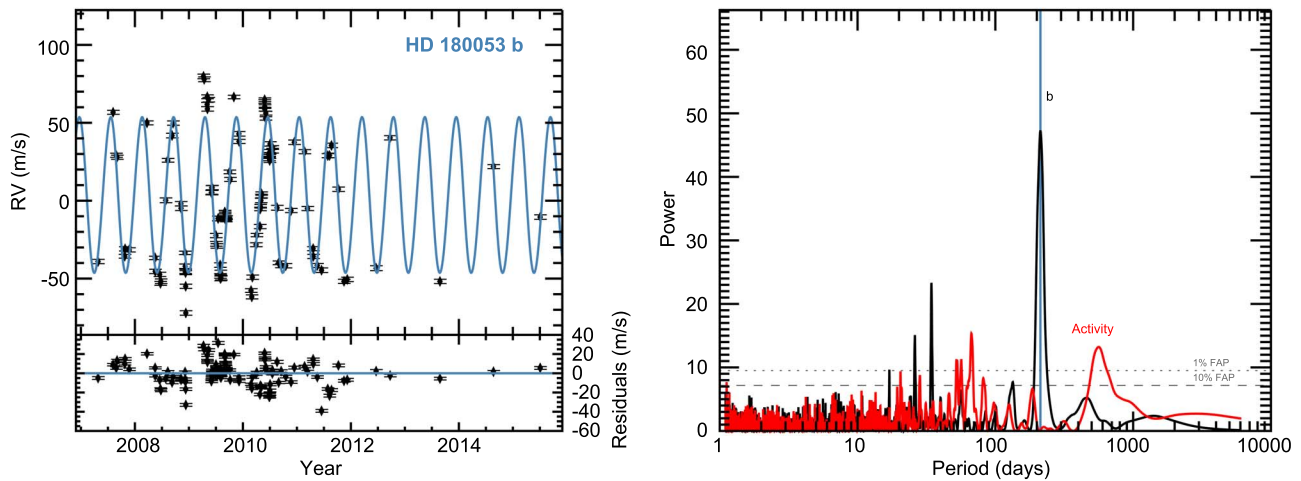
Figure 7. (Left) Time series of the best-fit orbital solution for HD 180053 b, which has period $P = 213.72$ days, eccentricity $e = 0.081$, and minimum mass $m_{\rm p} \sin i = 2.194~M_{\rm Jup}$. The residuals are shown in the bottom panel, which have an RV rms $= 13.8~{\rm m~s}^{-1}$, likely due to intrinsic variability induced by stellar activity. The remaining best-fit parameters can be found in Table 3. (Right) Periodogram of HD 180053 RV data before (black) and after (red) subtracting the best-fit planet parameters for HD 180053 b. The vertical line indicates the best-fit period of HD 180053 b. The remaining peaks in the periodogram are likely due to RV variations induced by stellar activity.
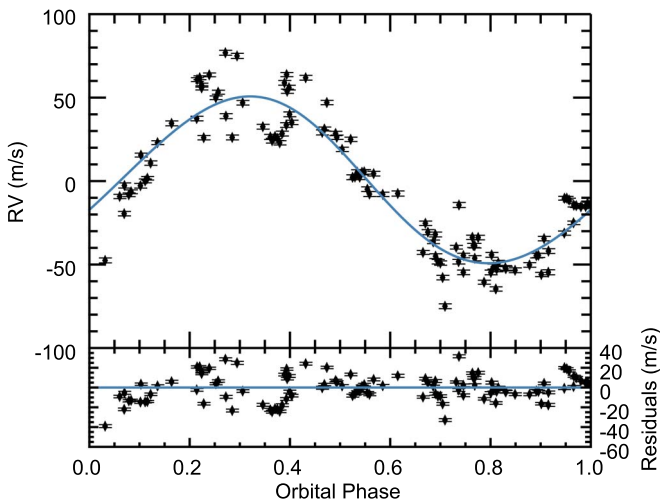
Figure 8. Phase-folded velocities of HD 180053 b.

improvement in the reduced χ^2 from 78 to 20 and finds HD 18742 c to have a period of 859 ± 41 days, eccentricity $e = 0.056 \pm 52$, and minimum mass $m_{\rm p} \sin i = 2.4 \pm 1.2~M_{\rm Jup}$. See Table 3 for more orbital and planet parameters and uncertainties. The time series for the second planet (HD 18742c) is shown in the left panel of Figure 12 with the full time series and two-planet fit shown in Figure 13.

Despite providing a much better fit and meeting all of our planet detection thresholds, we have listed it as a candidate signal because the resulting planet would be in a 9:10 resonance with the inner planet, which is nonphysical and would be the first set of planets in such a resonance. As a result, further scrutiny is needed in order to confirm or reject this planet. Given that the location of the periodogram peak is closer to 1000 days than 860 days (see Figure 12), it could simply be that we have found a shallow minimum in the two-planet fit that results in the unphysical resonance. Additional observations should uncover the true nature of this signal. Particularly, the one-planet and two-planet models reach their

largest divergence in mid-2018 (differ by $60~{\rm m~s}^{-1}$) and mid-2019 (differ by nearly $90~{\rm m~s}^{-1}$). Past observations mainly lie in regions where the two solutions differ by 10–$20~{\rm m~s}^{-1}$ with a few points out to 30–$40~{\rm m~s}^{-1}$ (all points more closely tracing the two-planet solution).

4.3. A Possible Third Planet around HD 163607

HD 163607 is a G5 IV star (Wenger et al. 2000) with two previously known planets (Giguere et al. 2012). It has a V magnitude $V = 7.979$, effective temperature $T_{\rm eff} = 5522$ K, and $\log g = 3.97$. It is a $1.12~M_\odot$ star with radius $1.76~R_\odot$. For additional stellar parameters and uncertainties, see Table 2. There are 73 RV observations of this star, the final 20 of which are additional points since the original discovery of HD 163607 b and c. All 73 RV observations come from Keck. After refitting the two planets and subtracting out the new best fits, there was a strong long-period signal in the periodogram, shown in the right panel of Figure 14. Refitting the time series with the inclusion of a third, long-period planet resulted in an improvement in the reduced χ^2 from 37 to 8. The time series for HD 163607 d is shown in Figure 14 with the full time series for all three planets shown in Figure 15. As is obvious from the time series, we have not covered a full orbit for this planet, which is why it is a planet candidate. We note that due to the long period of the planet and incomplete phase coverage, the derived orbital parameters for planet d are fairly uncertain, which will be resolved with future observations. In particular, the addition of the most recent observation (2018 September) has shown that the outer planet is indeed very long period and massive. Future observations will continue to constrain the outer planet, which in the current best fit has a mass $7.6 \pm 4.3~M_{\rm Jup}$, period $22{,}000 \pm 15{,}000$ days, and eccentricity 0.25 ± 0.25. Additional orbital parameters can be found in Table 3. If confirmed, this (or similarly HD 4917 above) will be the first three-planet system around a subgiant, which could be useful in determining evolutionary properties of planets around subgiant stars. The novelty of the three-planet subgiant system and probability of transit warrants its inclusion here despite lacking a fully constrained orbit.
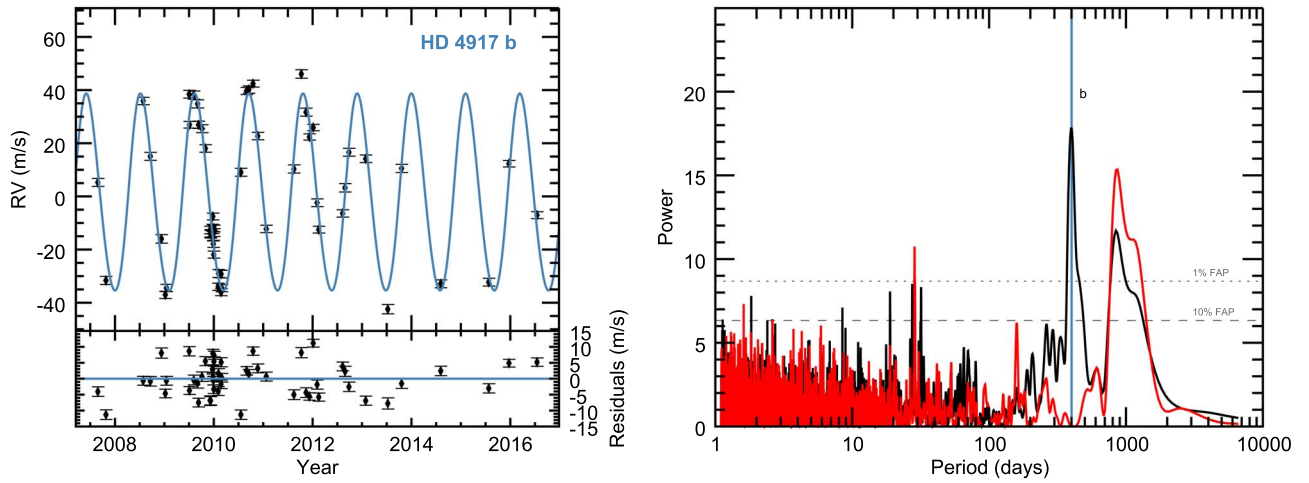
Figure 9. (Left) The isolated time series of HD 4917 b (period $P = 400.5 \pm 1.7$ days, eccentricity $e = 0.066 \pm 0.041$, and minimum mass $m_p \sin i = 1.615 \pm 0.093$ M_{Jup}). In this panel the signal from planet candidates c (period $P = 821 \pm 13$ days, eccentricity $e = 0.467 \pm 0.088$, and minimum mass $m_p \sin i = 1.37 \pm 0.13$ M_{Jup}) and d (period $P = 1093 \pm 37$ days, eccentricity $e = 0.28 \pm 0.14$, and minimum mass $m_p \sin i = 0.89 \pm 0.1 M_{Jup}$) have been subtracted out. (Right) Initial (black) and final (red) periodogram of HD 4917 after subtracting out the signal from planet b. The final periodogram shows the two peaks corresponding to planet candidates c and d.
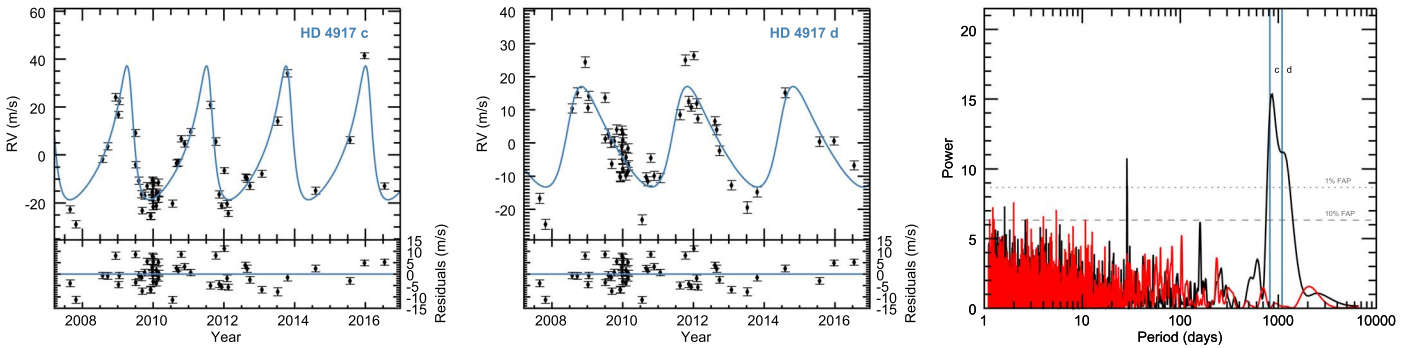
Figure 10. Two additional planet candidates around HD 4917. (Left) The isolated time series of HD 4917 c (period $P = 821 \pm 13$ days, eccentricity $e = 0.467 \pm 0.088$, and minimum mass $m_p \sin i = 1.37 \pm 0.13 M_{Jup}$). In this panel, the signals from planet b (period $P = 400.5 \pm 1.7$ days, eccentricity $e = 0.066 \pm 0.041$, and minimum mass $m_p \sin i = 1.615 \pm 0.093 M_{Jup}$) and planet candidate d (period $P = 1093 \pm 37$ days, eccentricity $e = 0.28 \pm 0.14$, and minimum mass $m_p \sin i = 0.89 \pm 0.1 M_{Jup}$) have been subtracted out. (Middle) The isolated time series of HD 4917 d with signals from planet b and planet candidate c subtracted out. (Right) Periodogram before (black) and after (red) subtracting out the two additional planet candidates HD 4917 c and d. In this case, the initial periodogram is after subtracting out planet b, and is identical to the red periodogram in Figure 9.
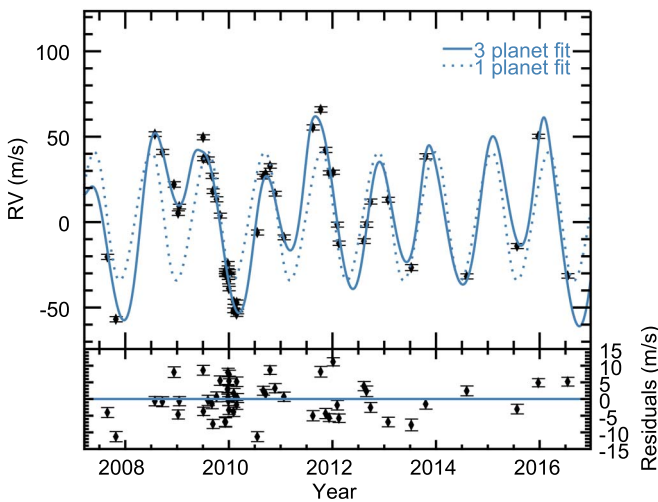

Figure 11. Full time series for HD 4917 and best three-planet fit compared to the best one-planet fit. A single planet does not fit well, especially evidenced by the observations between mid-2008 and mid-2010. The bottom panel shows the residuals to the three-planet fit.

4.4. A Possible Short-period Planet Orbiting HD 180902

HD 180902 is a K0 star (Wenger et al. 2000) with one previously known planet (Johnson et al. 2010b). Its V-band magnitude is $V = 7.78$, its effective temperature is $T_{eff} = 4961$ K, and it has a surface gravity $\log g = 3.36$. It has a mass of $1.41 M_\odot$ and radius $4.16 R_\odot$. The full list of stellar parameters and uncertainties is given in Table 2. There are 28 total RV observations for HD 180902, the final 17 of which are new observations that span over 6 yr since the original discovery of HD 180902 (Johnson et al. 2010b). It was noted in Johnson et al. (2010b) and later Bryan et al. (2016) that there was a long-term linear trend that was subtracted out, which was speculated to be a long-period companion. With the additional observations available since its discovery, we are now able to obtain a Keplerian signal to this trend. The trend is indeed due to a companion, which we estimate to be a low-mass star with minimum mass $98.7 \pm 7.6 M_{Jup}$. However, after performing this fit, an additional 15 day signal appeared in the periodogram. Fitting the system with three companions resulted in the best fit (bringing the reduced χ^2 from 12 in the two-companion
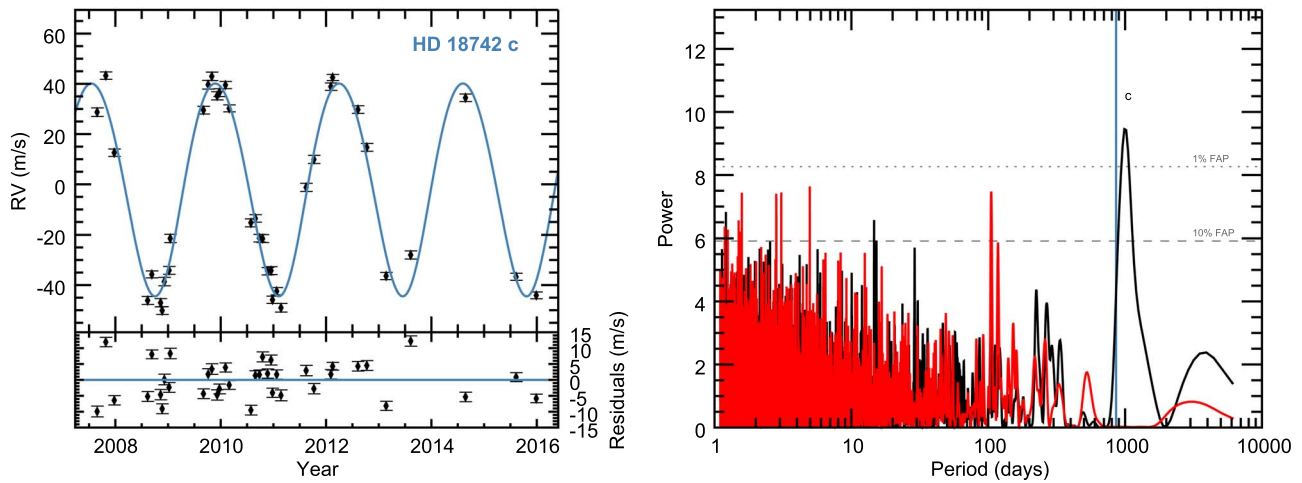
12

Figure 12. Residuals after subtracting out the previously discovered planet HD 18742 b (period $P = 766$ days, eccentricity $e = 0.040$, and minimum mass $m_p \sin i = 3.4 \, M_{\rm Jup}$), showing evidence of a second planet. (Left) Time series for HD 18742 c with period 859 days, eccentricity $e = 0.056$, and minimum mass $m_p \sin i = 2.4 \, M_{\rm Jup}$. (Right) Periodogram after subtracting out the best-fit orbital parameters for HD 18742 b (black) and after subtracting out the best two-planet fit (black). Note the peak in the black curve at about 900 days, the starting guess used in the two-planet fit. The vertical line of the best-fit planet period does not quite match the periodogram peak. This is likely due to the fact that the vertical line comes from the best-fit period of a two-planet joint fit, rather than simply a fit to the residuals of the first planet, which is shown in the periodogram. We note that the best two-planet fit results in an unphysical 9:10 resonance, which is why we consider HD 18742 c a planet candidate.
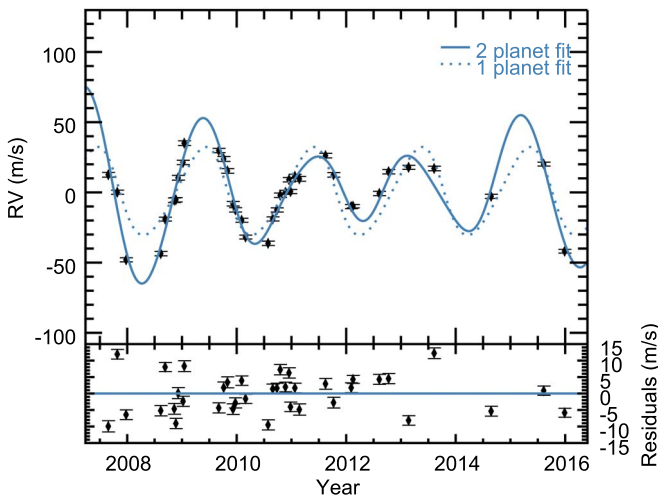
Figure 13. Full time series for HD 18742 and best two-planet fit. The dotted line shows for reference the best one-planet fit. The bottom panel shows the residuals to the two-planet fit. We note that the best two-planet fit results in an unphysical 9:10 resonance, which is why we consider HD 18742 c a planet candidate.

fit to 4 in the three-companion fit). With this fit, the system is therefore composed of two planets (HD 180902 A b,c), with a low-mass stellar companion (HD 180902 B). Like the long-period planet HD 163607 c, the phase coverage for stellar companion HD 180902 B is incomplete and so period and mass uncertainties are quite high. We expect this to be resolved as more observations are obtained. The periodogram showing the peak at 15 days for HD 180902 c is shown in the right panel of Figure 16, with the time series shown in the left panel. The phase curve for HD 180902 c is shown in Figure 17. HD 180902 c has a minimum mass roughly twice the mass of Neptune, at $0.099 \pm 0.014 \, M_{\rm Jup}$. Finally, the best-fit Keplerian signal for HD 180902 B is given in Figure 18, which shows the signal from HD 180902 B with the RV signals from HD 180902 b and c subtracted out. More phase coverage is needed

to place tighter constraints on the orbit of this companion. Orbital parameters for both stellar companion HD 180902 B and planet HD 180902 c are given in Table 3.

We have identified this planet as a planet candidate due to its high FAP, 1.2%. With the current observations, we are not fully convinced by the 15 day planet: the periodogram does not show a very strong signal, and the phase curve is sparsely sampled. Additionally, a 15 day period raises concerns of stellar rotation timescales and potentially activity-induced RV variations. Additionally, with a poorly constrained stellar binary, it is possible that this 15 day signal would be resolved simply with a more accurate fit to the stellar companion. With more observations, we should be able to confirm the existence of this planet. We further note that it has a relatively high transit probability. A detected transit, either ground-based or from *TESS*, would be able to confirm this planet, which is why we have included this candidate signal.

4.5. A Possible Sub-Jupiter Orbiting HD 196645

HD 196645 is a K0 subgiant with $V = 7.80$, $B - V = 0.91$ (Wenger et al. 2000). It has effective temperature $T_{\rm eff} = 5041$ K, and surface gravity $\log g = 3.43$. A summary of its stellar parameters can be found in Table 2.

It has 20 observations that span nearly 6 yr. The best-fit orbital solution yields a $m_p \sin i = 0.497 \pm 44 \, M_{\rm Jup}$ planet on a 128.94 ± 0.41 day period, with relatively low eccentricity, $e = 0.106 \pm 0.091$. The full set of orbital parameters are given in Table 3. Figure 19 shows the time series of HD 196645 b, with the initial and final periodogram for this system. For clarity, Figure 20 also shows the phase-folded velocities for HD 196645 b. For this star, the low semiamplitude and few observations keep us from definitively claiming this planet. It has FAP of 1.0% and is close to our $D > 10$ threshold at $D \sim 13.6$, which in combination lead to its candidate status. Continued observations will likely add significance to the periodogram peak and result in better phase coverage.
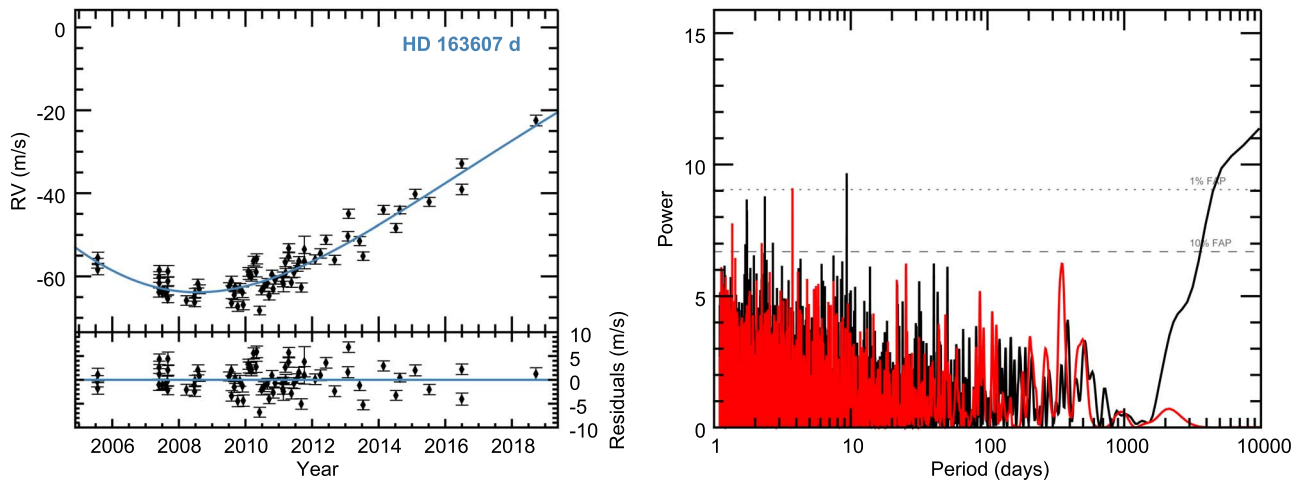
Figure 14. Residuals after subtracting out the two previously discovered planets HD 163607 b (period $P = 75.199$ days, eccentricity $e = 0.7502$, and minimum mass $m_p \sin i = 0.787 \, M_{Jup}$) and HD 163607 c (period $P = 1266.3$ days, eccentricity $e = 0.075$, and minimum mass $m_p \sin i = 2.193 \, M_{Jup}$), showing evidence of a third planet. (Left) Time series for HD 163607 d with period 22000 ± 15000 days, eccentricity 0.25 ± 0.25, and minimum mass $7.6 \, M_{Jup}$. Incomplete phase coverage means that the uncertainty in the period and eccentricity is relatively high. (Right) Periodogram after subtracting out the best-fit orbital parameters for HD 163607 b and c (black) and the final periodogram after subtracting out planet d in the best three-planet fit (red). Planet d is seen as a wide peak at long periods, extending beyond the plot.
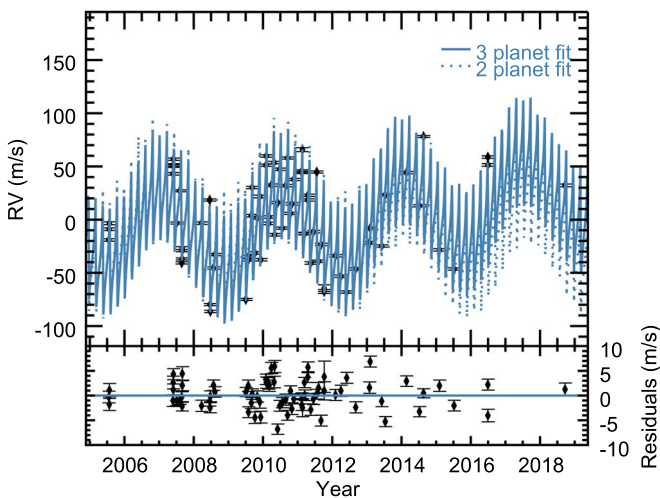

Figure 15. Full time series for HD 163607 and best three-planet fit. The new planet, HD 163607 d is the long-period trend that reaches minimum around 2009 and maximum in 2016, evident by the differing minima of the 1000 day planet). The difference between the two- and three-planet fits is not as easily seen in the time series. The bottom panel shows the residuals to the three-planet fit.

4.6. A Possible Jupiter Orbiting HD 207077

HD 207077 is a G8 subgiant with $V = 8.24$, $B - V = 0.870$ (Wenger et al. 2000). It has effective temperature $T_{eff} = 5067$ K, and surface gravity $\log g = 3.27$. A summary of its stellar parameters can be found in Table 2.

It has observations starting in 2007 that span roughly 8 yr. HD 207077 was previously identified in Butler et al. (2017) as having a planet candidate. The best-fit orbital solution yields a $m_p \sin i = 1.16 \pm 0.10 \, M_{Jup}$ planet on a 606.3 ± 3.8 day period, with eccentricity, $e = 0.204 \pm 0.099$. The full set of orbital parameters are given in Table 3. Figure 21 shows the time series of HD 207077 b, with the initial and final periodogram for this system. Despite passing all of our planet detection thresholds, we are conservative for this star due to

poor phase coverage and have classified it as a candidate. Continued observations will likely add to the periodogram peak and result in better phase coverage and confirm the planet status. We additionally note that this star has a relatively high RV rms compared to similar stars (J. K. Luhn et al. 2018, in preparation). Comparing the expected level of stellar jitter from similar stars to the measured RV rms for this star indicates further evidence for an unsubtracted planet in the data that is responsible for the artificially high RV rms.

4.7. A Possible Additional Planet Orbiting HD 33142

HD 33142 is a K0 subgiant (Wenger et al. 2000) with one previously known planet (Johnson et al. 2011). It has a V magnitude $V = 7.96$, $B - V = 0.945$, effective temperature $T_{eff} = 4978$ K, and $\log g = 3.40$. It has a mass of $1.41 \, M_\odot$. Additional stellar properties can be found in Table 2. There are 40 observations spanning about 8 yr, and we make use of the additional seven points since the initial publication. The original fit for this planet in Johnson et al. (2011) noted unusually high jitter in this star and claimed evidence of a planet near 900 days, which we show in the periodogram with the residuals to our best fit to HD 33142 b in the right panel of Figure 22 . As can be seen, we find evidence for a second planet near 800 days. Refitting the RVs with a two-planet fit starting with a second planet near 800 days resulted in an improvement in the reduced χ^2 from 38 to 19. The minimum mass for HD 33142 c is $0.59 \pm 0.10 \, M_{Jup}$ and it has a period of 809 days and eccentricity $e = 0.16$. See Table 3 for more orbital and planet parameters and uncertainties. The time series for the second planet (HD 33142c) is shown in Figure 22 with the full time series and two-planet fit shown in Figure 23. This planet candidate does not meet our detection threshold $D > 10$ with $D = 9.4$. Additionally, it is not clear from the phase curve nor the full time series that the second planet is indeed present and with further observations we should know for certain.

5. Nonplanetary Companions to Subgiant Stars

A number of stars in our sample of subgiants showed evidence of stellar binary companions ($m \sin i > 13 \, M_{Jup}$). All
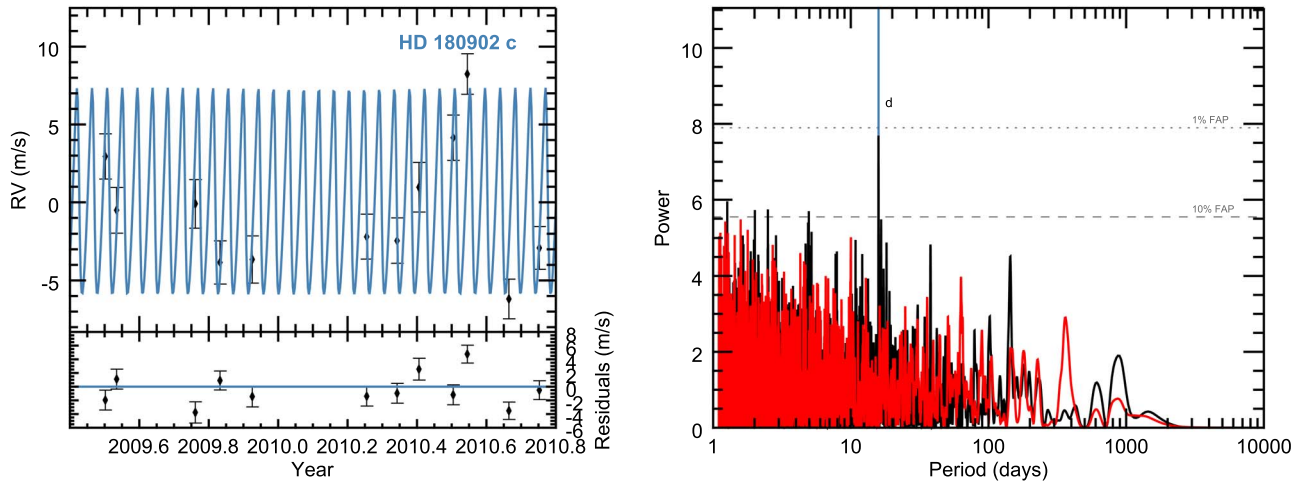
Figure 16. Residuals after subtracting out the previously discovered planet HD 180902 b (period $P = 510.9$ days, eccentricity $e = 0.107$, and minimum mass $m_p \sin i = 1.685\ M_{\mathrm{Jup}}$) and the best-fit Keplerian for the stellar binary HD 180902 B (period $P = 5880$ days, eccentricity $e = 0.107$, and minimum mass $m_p \sin i = 98.7\ M_{\mathrm{Jup}}$), showing evidence of a second planet. (Left) Time series for HD 180902 c with period 15.9058 days, eccentricity $e = 0.28$, and minimum mass $m_p \sin i = 0.099\ M_{\mathrm{Jup}}$. Due to the short period, the time series on the left has been zoomed in on a high-density region of observations, but Figure 18 shows the full set of observations for this star with the longer period stellar binary companion. The phase curve for this planet is shown in Figure 17. (Right) Periodogram before (black) and after (red) subtracting the 15 day signal for HD 180902 c.
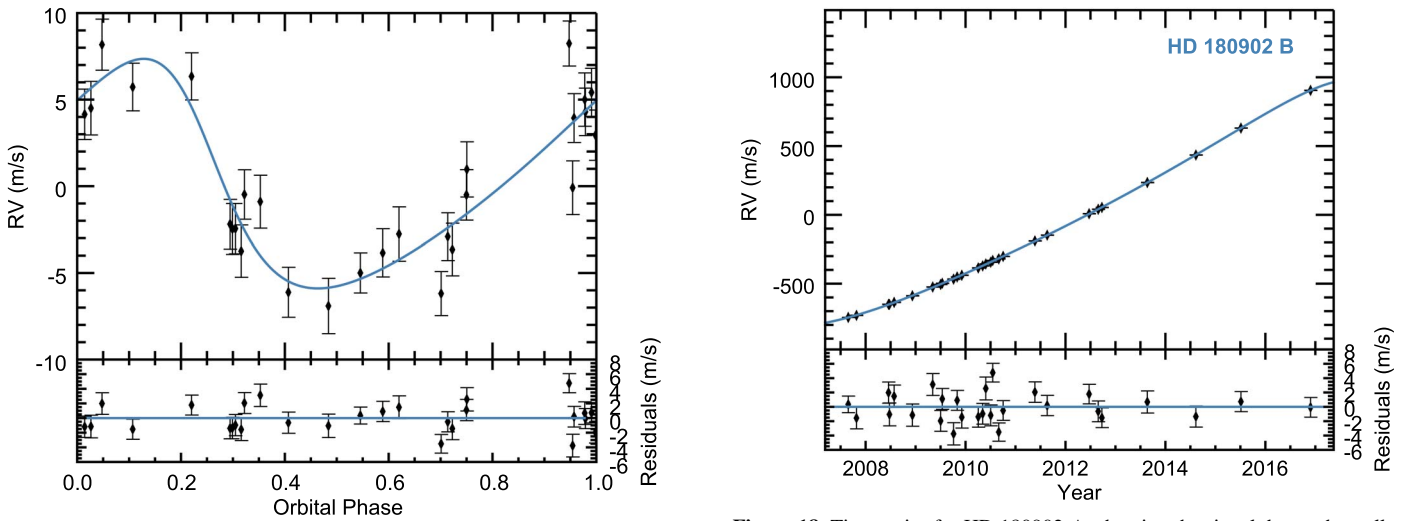

Figure 17. Phase curve for HD 180902 c with period 15 days.

Figure 18. Time series for HD 180902 A, showing the signal due to the stellar companion HD 180902 B, where the signals from HD 180902 b and c have been subtracted out. Here we show that the previously identified linear trend has some curvature and can be fit by a Keplerian with period 5880 days; however, the phase coverage is incomplete, so errors for estimated parameters are large. For now, it appears to be a low-mass star or brown dwarf.

binaries are listed in Table 3 and their time series can be seen in Figure 24. In the following paragraphs, we describe those with minimum mass less than 100 M_{Jup}, as these are likely brown dwarf candidates and of special interest to the exoplanet community.

5.1. A 22 M_{Jup} Brown Dwarf Orbiting HD 125390

HD 125390 is a G7 star (Wenger et al. 2000) with V-band magnitude 8.21, effective temperature $T_{\mathrm{eff}} = 4850$ K, and surface gravity $\log g = 3.13$. It has a mass of 1.12 $M_\odot$ and has 15 observations over a 6 yr span. We present the discovery of a 22.16 ± 0.96 M_{Jup} brown dwarf companion to this star with period 1756.2 ± 3.9 days. The rest of the orbital parameters can be found in Table 3. The time series for this companion is shown in Figure 24.

5.2. HD 148284

HD 148284 is a K0 star (Wenger et al. 2000) with V-band magnitude 9.01, effective temperature $T_{\mathrm{eff}} = 5572$ K, and surface gravity $\log g = 3.97$. It has a mass of 1.02 $M_\odot$ and has 30 observations over an 11 yr span. We present the discovery of a 34.5 ± 0.96 M_{Jup} brown dwarf companion to this star with period 339.302 ± 0.026 days. The rest of the orbital parameters can be found in Table 3. The time series for this companion is shown in Figure 24.

5.3. HD 214823

HD 214823 is a G0 star (Wenger et al. 2000) with V-band magnitude 8.07, effective temperature $T_{\mathrm{eff}} = 5933$ K, and
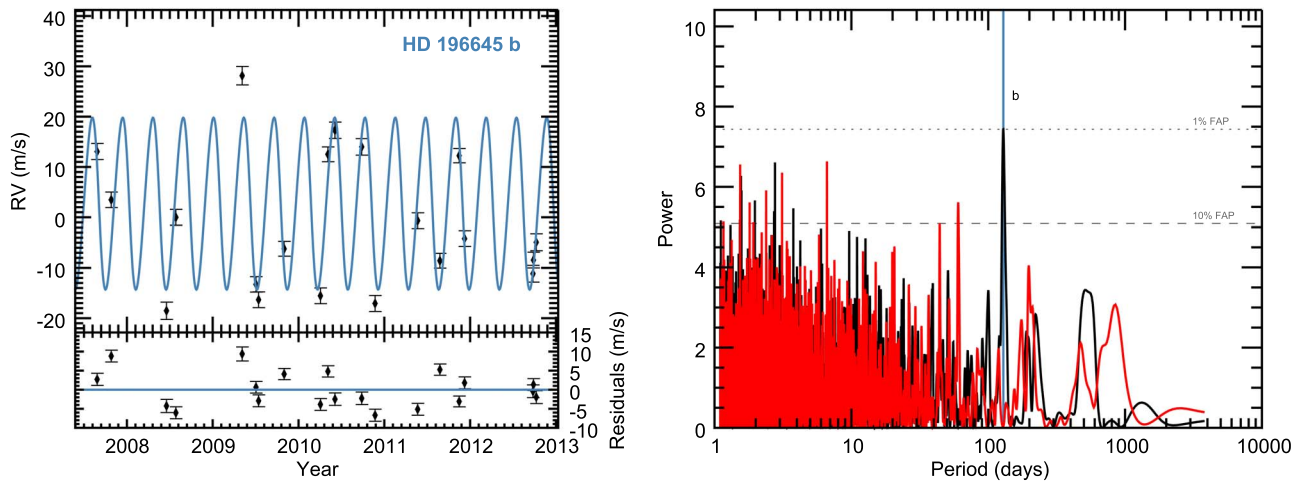
Figure 19. (Left) Time series and best-fit orbital solution for HD 196645 b, with a 128.94 day period, eccentricity 0.106, and minimum mass 0.497 $M_{\rm Jup}$. The residuals are shown in the bottom panel, which have an RV rms = 4.7 m s^{-1}. The remaining best-fit parameters can be found in Table 3. The phase curve can be seen in Figure 20. (Right) Periodogram of HD 196645 RV data before (black) and after (red) subtracting the best-fit planet parameters for HD 196645 b. The vertical line indicates the best-fit period of HD 196645 b.
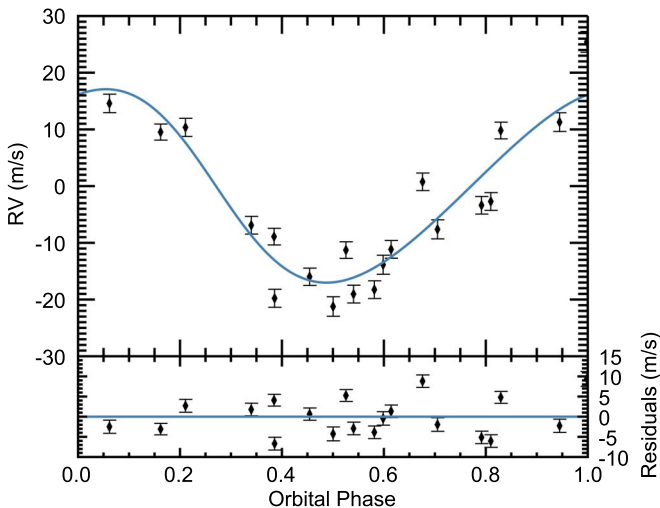

Figure 20. Phase-folded velocities of the best-fit solution for HD 196645 b.

surface gravity $\log g = 3.92$. It has a mass of 1.31 $M_\odot$ and has 28 observations over an 11 yr span. We present the discovery of a 20.56 ± 0.32 $M_{\rm Jup}$ brown dwarf companion to this star with period 1853.9 ± 1.6 days. The rest of the orbital parameters and uncertainties can be found in Table 3. The time series for this companion is shown in Figure 24.

5.4. Brown Dwarf Candidate Orbiting HD 180902

We have already remarked on this system in Section 4.4; however, we wish to make a final remark here. The minimum mass for the stellar companion HD 180902 B (98.7 ± 7.6 $M_{\rm Jup}$) places it in as a candidate brown dwarf. However, the orbit for this companion is poorly constrained and so it is likely that the mass could substantially change with continued observations.

6. Transit Times, Probabilities, Depths, and Durations of CPS Subgiants with Known RV Planets

Here we describe the transit parameters for subgiant companions used in this work, all of which are are given in Table 5. At typical separations of planets in this paper (1–2 au),

the average value for the transit probability is roughly 2.2%.[12] For the 60 planets in Table 5 it is likely that 1 or 2 will in fact transit. Observing a planet in transit provides a wealth of additional information about the system, most notably the size and mass (without the $\sin i$ dependence) of the planet, which provides a bulk density for the planet. As an example, KELT-11 b (also referred to as HD 93396) is a highly inflated planet —which we know only because we have mass and radius information from the combined RV and transit data—on a short-period orbit around a subgiant star (Pepper et al. 2017). With transit observations of RV planets on similarly close orbits around subgiants we can understand how unique inflated planets like KELT-11 b are and whether the increased insolation from the evolved subgiant host plays a role in inflating the planet. Furthermore, transits provide a model-independent measure of the stellar density, which combined with the radius from parallax would produce a model-independent stellar mass (Seager & Mallén-Ornelas 2003). Using *Gaia* parallaxes, reasonable SED measurements, and precise transits, errors in the stellar radius would be 1%, and mass errors 3% (Beatty et al. 2017).

In order to determine the best transit parameters, we refit all RV data for known subgiants. The reasons for this were two-fold: (1) several of these planets have additional observations since their published discovery, and (2) updated stellar parameters from Brewer et al. (2016) allow for more accurate planet masses and reduced uncertainties in predicted transit time durations. All best-fit orbital parameters in this work were obtained using the IDL RVLIN package (Wright et al. 2009) in conjunction with the BOOTTRAN (Wang et al. 2012) package, which works with RVLIN and uses the bootstrapping technique to find best-fit parameters and uncertainties of RV fits. The best-fit orbital solutions for each planet is given in Table 3 and we include all RV observations used in this work in Table 4. Once we fit the RV data and obtained new orbital parameters, the final remaining step was to estimate radii in order to calculate estimated transit parameters. We used the Python

---

[12] We have excluded binary companions and only included planet companions in this rough calculation. We have also done a literature search for detections of transits (null or positive) for those in our sample with transit probability >10% and have removed those from this calculation.
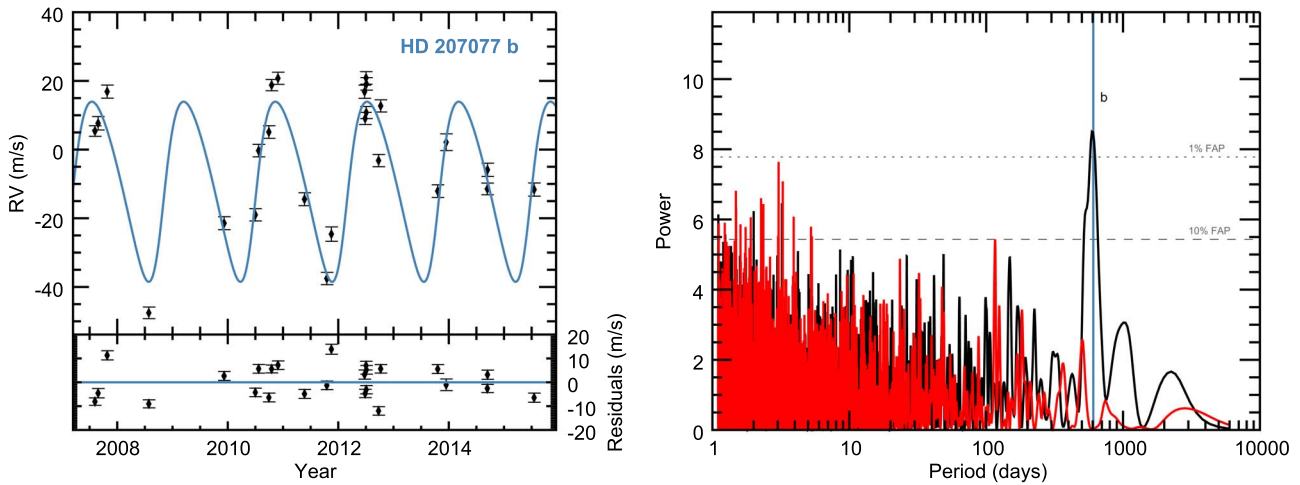
Figure 21. (Left) Time series and best-fit orbital solution for HD 207077 b, which has period $P = 606.3$ days, eccentricity $e = 0.204$, and minimum mass $m_p \sin i = 1.16$ M_{Jup}. The residuals are shown in the bottom panel, which have an RV rms = 6.7 m s^{-1}. The remaining best-fit parameters can be found in Table 3. (Right) Periodogram of HD 207077 RV data before (black) and after (red) subtracting the best-fit planet parameters for HD 207077 b. The vertical line indicates the best-fit period of HD 207077 b.
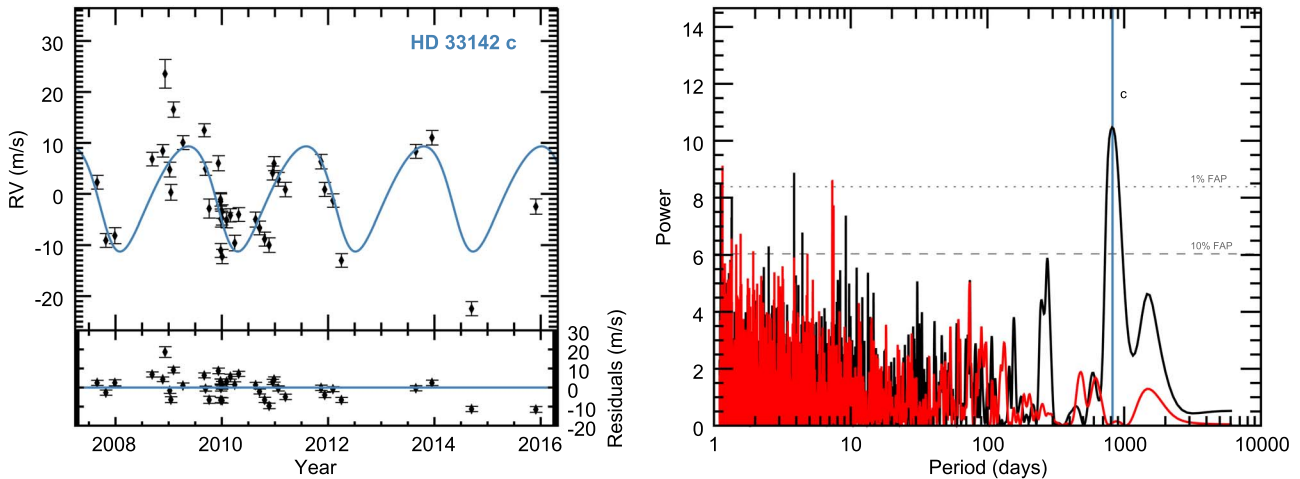

Figure 22. Residuals after subtracting out the previously discovered planet HD 33142 b (period $P = 326.0$ days, eccentricity $e = 0.066$, and minimum mass $m_p \sin i = 1.306$ M_{Jup}), showing evidence of a second planet. (Left) Time series for HD 33142 c with period 809 days, eccentricity $e = 0.16$, and minimum mass $m_p \sin i = 0.59$ M_{Jup}. (Right) Periodogram after subtracting out the best-fit orbital parameters for the previously discovered planet HD 33142 b (black) and the final periodogram after subtracting out the best two-planet fit (red). Note the black peak at 800 days, the starting guess used in the two-planet fit.

code FORECAST (Chen & Kipping 2017) to estimate radii from minimum masses provided by the RV fits. We note that our transit calculations are meant to be estimates and, as such, we merely used the mean radius from FORECAST and do not include radius errors.[13] The BOOTTRAN package also outputs the Barycentric Julian Date (BJD) of the next n times of inferior conjunction and their uncertainties. For simplicity we use the terms "conjunction time" and "transit time" synonymously despite the fact that the planet may not actually transit. Using BOOTTRAN, we predict the next three transits for each planet starting after 2018 October 1 and report those with uncertainties as carried through by BOOTTRAN in Julian Date (columns 3–8). They require space-based observations because the majority of these planets are at 1–2 au around inflated subgiants so their transit depths will likely be difficult to observe with ground-based telescopes, and transit durations and ingress/egress durations will be rather long, again posing a difficulty for ground-based transits. Despite the short

---

[13] Typical radius errors were 0.2 R_{Jup}, which results in less than 0.01% uncertainty in the transit probabilities.
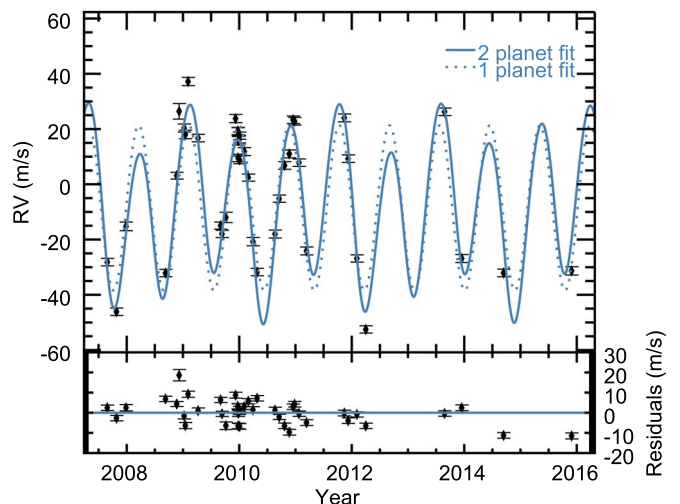

Figure 23. Full time series for HD 33142 and best two-planet fit. The dotted line shows for reference the best one-planet fit. The bottom panel shows the residuals to the best two-planet fit.
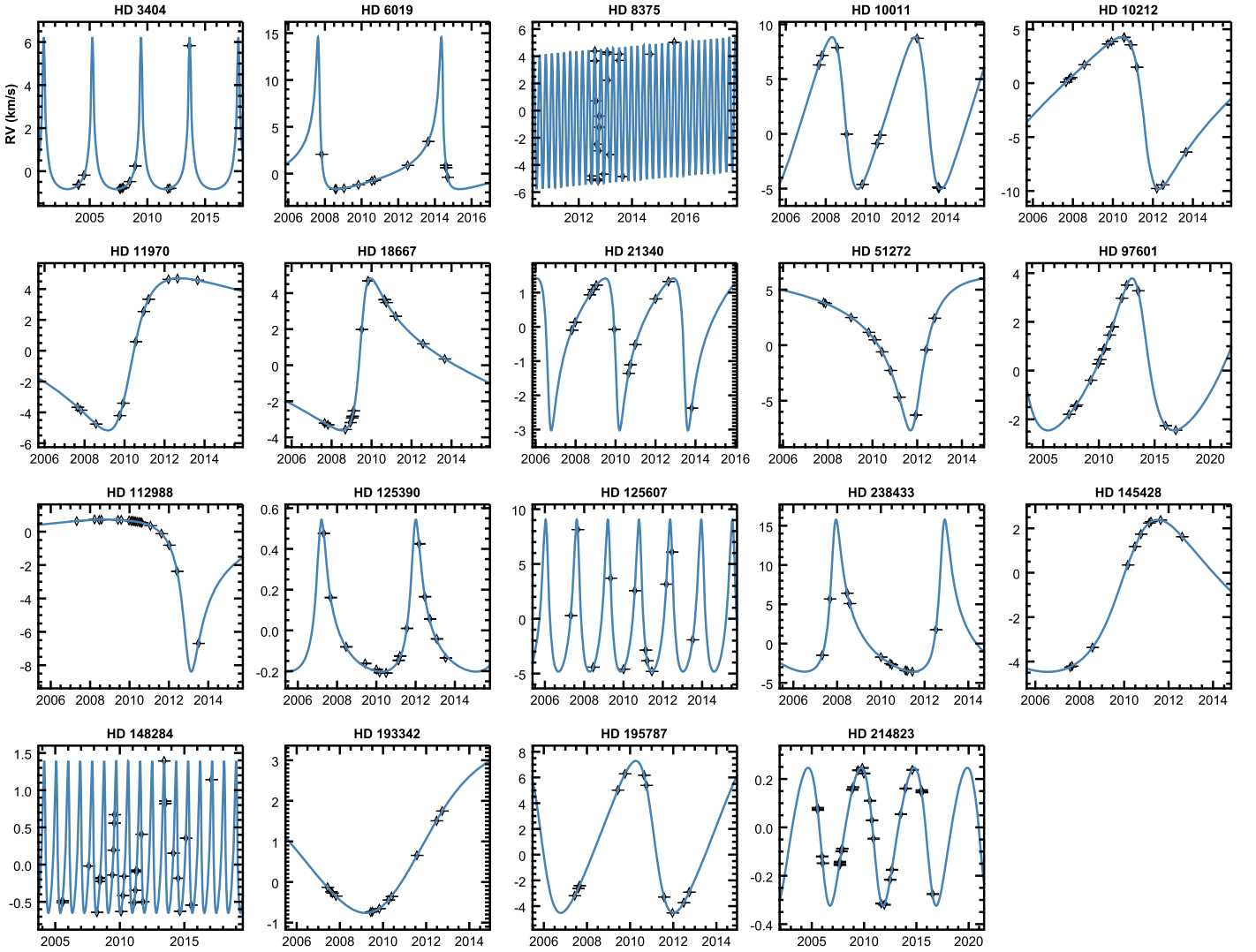
Figure 24. Full time series for all stellar binaries in this work. Best-fit orbital parameters for each system can be found in Table 3. Note that the *y*-axes have units of kilometers per second. Vertical error bars are added for clarity as in previous figures. The horizontal marks do not show error in time.

Table 4
Radial Velocities

Star	Date (JD-2440,000)	RV (m s^{-1})	σ_{RV} (m s^{-1})	Tel
(1)	(2)	(3)	(4)	(5)
HD 10697	10367.062	−35.57	1.28	Keck
HD 10697	10461.806	−90.39	1.22	Keck
HD 10697	10715.068	−104.39	1.17	Keck
HD 10697	10716.098	−103.92	1.17	Keck
HD 10697	10806.863	−43.35	1.25	Keck
HD 10697	10837.732	−37.86	1.37	Keck
HD 10697	10838.708	−31.17	1.07	Keck

(This table is available in its entirety in machine-readable form.)

photometric baseline from surveys like *TESS* (∼27 days for the shortest), they may manage to catch one of these planets in transit. Furthermore, the longer period RV planets have large uncertainties on their predicted transit times, which would pose further problems for ground-based observing. We calculate the transit parameters as given in Seager (2010), including the full a priori transit probability

$$\tau_{pr} = \frac{(R_\star + R_p)}{a} \frac{(1 + e \sin \omega)}{1 - e^2}, \tag{2}$$

(see also Seagroves et al. 2003; Barnes 2007) which is given in column 9. True a posteriori probabilities (Stevens & Gaudi 2013) can be computed with knowledge of the underlying mass function for planets orbiting subgiants with comparable periods and host star masses. Since the exoplanet mass function has negative slope, this means our transit probabilities as given in Equation (2) are slightly underestimated. The transit depth is simply

$$\tau_{depth} = \left(\frac{R_p}{R_\star}\right)^2 \tag{3}$$

and is given in column 10. We also calculate transit and ingress/egress durations, which are given by

$$\tau_{dur} = \frac{P}{\pi} \arcsin\left(\frac{R_\star}{a\sqrt{\left(1 + \frac{R_p}{R_\star}\right)^2}}\right). \tag{4}$$

Table 5
Transit Parameters for Known Planets around Subgiants

Star	Com	τ_1 (JD)	σ_1 (JD)	τ_2 (JD)	σ_2 (JD)	τ_3 (JD)	σ_3 (JD)	τ_{pr} (%)	τ_{depth} (ppm)	τ_{dur} (hr)	$\Delta\tau_{12}$ (hr)	τ_1 (yyyy mm dd)	τ_2 (yyyy mm dd)	τ_3 (yyyy mm dd)
(1)	(2)	(3)	(4)	(5)	(6)	(7)	(8)	(9)	(10)	(11)	(12)	(13)	(14)	(15)
HD 10697	b	2458961.13	6.46	2460036.82	7.17	2461112.51	7.91	0.46	4360.578	30.9724	1.9186	2020 Apr 21	2023 Apr 2	2026 Mar 13
HD 38529[a]	b	2458405.55	0.12	2458419.86	0.12	2458434.17	0.12	13.44[a]	2582.275	7.9461	0.3837	2018 Oct 14	2018 Oct 28	2018 Nov 11
⋯	c	2458889.11	6.20	2461025.19	9.31	2463161.28	12.42	0.43	2023.902	47.3599	2.0389	2020 Feb 9	2025 Dec 15	2031 Oct 21
HD 114613	b	2458570.08	194.59	2462572.23	288.82	2466574.38	394.43	0.22	3208.864	61.2665	3.2845	2019 Mar 27	2030 Mar 11	2041 Feb 23
HD 117176	b	2458457.10	0.18	2458573.79	0.18	2458690.48	0.19	2.31	3843.355	15.8918	0.9276	2018 Dec 4	2019 Mar 31	2019 Jul 25
HD 159868	b	2458487.74	24.49	2459671.82	31.03	2460855.89	37.79	0.46	3349.915	40.0036	2.1887	2019 Jan 4	2022 Apr 2	2025 Jun 29
⋯	c	2458662.80	12.74	2459013.76	13.50	2459364.73	14.29	0.86	3738.315	32.9151	1.8965	2019 Jun 28	2020 Jun 13	2021 May 30
HD 175541	b	2458484.93	8.74	2458783.36	9.10	2459081.79	9.48	2.26	977.176	43.0429	1.3046	2019 Jan 1	2019 Oct 26	2020 Aug 20
HD 190228	b	2459235.07	5.57	2460378.57	7.12	2461522.06	8.68	1.23	2271.500	25.5255	1.1612	2021 Jan 20	2024 Mar 9	2027 Apr 26
HD 1502	b	2458557.95	10.45	2458986.43	11.52	2459414.90	12.61	1.81	675.349	56.3972	1.4284	2019 Mar 15	2020 May 16	2021 Jul 19
HD 3404	*	2459669.59	5.87	2461213.13	5.68	2462756.66	5.55	0.85	7472.735	29.4967	2.3470	2022 Mar 31	2026 Jun 21	2030 Sep 12
HD 4313	b	2458725.41	8.63	2459081.63	9.47	2459437.84	10.33	2.47	584.958	49.8151	1.1763	2019 Aug 29	2020 Aug 20	2021 Aug 11
HD 5319	b	2458827.91	10.46	2459465.05	11.69	2460102.20	12.93	1.30	961.450	58.1012	1.7473	2019 Dec 10	2021 Sep 7	2023 Jun 6
⋯	c	2459200.27	18.50	2460072.48	23.85	2460944.69	29.46	0.87	1004.424	78.9995	2.4268	2020 Dec 16	2023 May 7	2025 Sep 26
HD 5608	b	2458994.82	28.82	2459774.69	33.12	2460554.56	37.51	1.22	594.445	80.4063	1.9137	2020 May 25	2022 Jul 14	2024 Sep 1
HD 6019	*	2459283.41	0.34	2461740.42	0.33	2464197.42	0.42	2.91	7244.043	51.6680	4.0526	2021 Mar 9	2027 Nov 30	2034 Aug 22
HD 8375	*	2458434.53	0.23	2458518.50	0.24	2458602.47	0.25	4.11	2293.321	26.8375	1.2261	2018 Nov 12	2019 Feb 3	2019 Apr 28
HD 10011	*	2459367.22	3.64	2460885.54	4.80	2462403.86	5.96	1.12	19522.233	65.4003	8.0175	2021 Jun 1	2025 Jul 29	2029 Sep 24
HD 10212	*	2459097.32	14.84	2462450.28	30.39	2465803.25	45.95	1.00	22553.972	74.5061	9.7283	2020 Sep 4	2029 Nov 9	2039 Jan 14
HD 10442	b	2458803.59	37.22	2459835.89	43.99	2460868.18	51.44	0.43	4105.661	43.7453	2.6342	2019 Nov 16	2022 Sep 13	2025 Jul 11
HD 11970	*	2461234.25	114.19	2469737.55	253.50	2478240.86	392.64	0.16	23684.597	266.2444	35.5096	2026 Jul 12	2049 Oct 23	2073 Feb 2
HD 13167	b	2460962.95	98.75	2463575.46	98.45	2466187.97	101.56	0.18	2509.603	106.8638	5.0980	2025 Oct 14	2032 Dec 8	2040 Feb 3
HD 14787	b	2458429.05	45.36	2459105.65	52.84	2459782.24	60.41	1.38	655.045	75.1774	1.8760	2018 Nov 6	2020 Sep 13	2022 Jul 21
HD 18015	b	2460468.05	152.62	2462746.29	217.80	2465024.54	285.76	0.34	1471.475	78.8912	2.9144	2024 Jun 6	2030 Sep 1	2036 Nov 27
HD 18667	*	2460779.46	13.81	2465155.06	26.48	2469530.66	39.24	0.25	6995.873	252.0085	19.4513	2025 Apr 13	2037 Apr 6	2049 Mar 30
HD 18742	b	2458913.70	86.02	2459680.11	110.79	2460446.53	136.03	1.34	543.356	79.2323	1.8048	2020 Mar 5	2022 Apr 10	2024 May 16
⋯	c	2458828.96	968.46	2459687.69	1004.79	2460546.41	1041.14	1.22	569.978	83.5374	1.9478	2019 Dec 11	2022 Apr 18	2024 Aug 23
HD 21340	*	2458942.89	6.76	2460192.58	9.24	2461442.27	11.71	2.40	645.813	63.2127	1.5666	2020 Apr 3	2023 Sep 5	2027 Feb 5
HD 28678	b	2458525.45	13.23	2458905.67	14.72	2459285.90	16.23	2.97	377.848	66.7229	1.2721	2019 Feb 10	2020 Feb 26	2021 Mar 12
HD 30856	b	2458419.15	61.31	2459266.62	80.60	2460114.09	100.08	1.16	819.205	72.9918	2.0310	2018 Oct 27	2021 Feb 21	2023 Jun 18
HD 33142	b	2458542.97	12.35	2458868.93	13.42	2459194.88	14.52	2.03	844.941	46.7382	1.3201	2019 Feb 28	2020 Jan 20	2020 Dec 11
⋯	c	2459201.07	224.26	2460009.99	485.33	2460818.91	677.24	1.23	903.456	57.6308	1.6817	2020 Dec 17	2023 Mar 6	2025 May 23
HD 38801	b	2458945.18	8.46	2459631.94	9.74	2460318.70	11.06	0.67	2330.606	39.2068	1.8056	2020 Apr 5	2022 Feb 21	2024 Jan 9
HD 45410	b	2459029.89	33.20	2459964.16	41.37	2460898.43	49.72	1.24	568.684	79.0858	1.8420	2020 Jun 29	2023 Jan 19	2025 Aug 10
HD 51272	*	2461027.52	664.54	2466686.99	1340.99	2472346.45	2017.44	0.65	13116.036	210.3041	21.6101	2025 Dec 18	2041 Jun 16	2056 Dec 13
HD 72490	b	2459092.41	50.54	2459950.47	61.31	2460808.53	72.24	1.37	634.563	76.3301	1.8755	2020 Aug 30	2023 Jan 5	2025 May 13
HD 73534	b	2458536.19	66.60	2460286.17	88.79	2462036.14	111.76	0.44	2472.393	54.5783	2.5853	2019 Feb 21	2023 Dec 7	2028 Sep 21
HD 75784	b	2458550.23	12.45	2458891.42	13.36	2459232.62	14.29	1.58	1441.043	42.0341	1.5372	2019 Mar 7	2020 Feb 11	2021 Jan 18
⋯	c	2464151.96	6775.66	2472003.35	9117.63	2479854.75	11295.54	0.18	1226.221	142.9796	4.8374	2034 Jul 8	2056 Jan 5	2077 Jul 5
HD 88133[a]	b	2458395.69	0.04	2458399.10	0.04	2458402.52	0.04	22.89[a]	2376.247	5.7657	0.2657	2018 Oct 4	2018 Oct 7	2018 Oct 11
HD 93396[b]	b	2458392.98	0.18	2458397.71	0.18	2458402.45	0.18	25.65[b]	964.937	6.7779	0.2026	2018 Oct 1	2018 Oct 6	2018 Oct 11
HD 94834	b	2459431.40	174.81	2461007.85	249.29	2462584.30	324.60	0.81	920.072	80.7779	2.3781	2021 Aug 4	2025 Nov 28	2030 Mar 23
HD 95089	b	2459086.08	63.01	2460870.86	93.21	2462655.64	123.93	1.00	553.833	75.5569	1.7372	2020 Aug 24	2025 Jul 14	2030 Jun 3
⋯	c	2458827.04	205.76	2459291.39	208.43	2459755.75	211.27	1.63	628.965	70.1498	1.7162	2019 Dec 9	2021 Mar 17	2022 Jun 25
HD 96063	b	2458607.90	35.45	2458970.42	37.29	2459332.94	39.18	1.76	719.066	67.4129	1.7604	2019 May 4	2020 Apr 30	2021 Apr 28
HD 96167	b	2458688.67	28.19	2459186.71	28.67	2459684.75	29.14	0.49	4524.795	56.1604	3.5396	2019 Jul 24	2020 Dec 3	2022 Apr 15
HD 97601	*	2460937.49	442.33	2465078.54	834.37	2469219.59	1227.61	0.56	6822.725	93.2152	7.1121	2025 Sep 18	2037 Jan 20	2048 May 23
HD 98219	b	2458637.96	14.02	2459071.72	15.83	2459505.49	17.68	1.75	728.688	57.9542	1.5232	2019 Jun 3	2020 Aug 10	2021 Oct 17
HD 99706	b	2458729.97	135.98	2459571.05	167.00	2460412.13	198.52	1.69	534.082	69.4327	1.5683	2019 Sep 3	2021 Dec 22	2024 Apr 11
HD 102956	b	2458393.61	0.09	2458400.11	0.09	2458406.60	0.09	26.16	807.999	13.9966	0.3821	2018 Oct 2	2018 Oct 8	2018 Oct 15
HD 106270	b	2458868.48	31.51	2460756.22	45.92	2462643.96	60.93	0.41	1913.123	54.3065	2.2758	2020 Jan 19	2025 Mar 21	2030 May 22
HD 108863	b	2458503.72	22.95	2458941.38	25.67	2459379.04	28.42	2.06	455.595	69.6541	1.4556	2019 Jan 20	2020 Apr 1	2021 Jun 13

Table 5
(Continued)

Star (1)	Com (2)	τ_1 (JD) (3)	σ_1 (JD) (4)	τ_2 (JD) (5)	σ_2 (JD) (6)	τ_3 (JD) (7)	σ_3 (JD) (8)	τ_{pr} (%) (9)	τ_{depth} (ppm) (10)	τ_{dur} (hr) (11)	$\Delta\tau_{12}$ (hr) (12)	τ_1 (yyyy mm dd) (13)	τ_2 (yyyy mm dd) (14)	τ_3 (yyyy mm dd) (15)
HD 112988	*	2461931.23	512.60	2467708.70	1034.71	2473486.17	1556.84	1.11	4836.263	96.7614	6.2916	2028 Jun 8	2044 Apr 3	2060 Jan 27
HD 125390	*	2459610.29	11.10	2461366.53	13.24	2463122.77	16.01	1.23	293.634	127.7546	2.1523	2022 Jan 30	2026 Nov 22	2031 Sep 13
HD 125607	*	2458440.62	0.65	2459019.16	0.75	2459597.70	0.86	1.91	8429.183	50.7931	4.2711	2018 Nov 18	2020 Jun 18	2022 Jan 18
HD 131496	b	2458858.64	64.26	2459755.11	79.51	2460651.58	94.89	1.26	790.488	61.8007	1.6900	2020 Jan 10	2022 Jun 24	2024 Dec 7
HD 238433	*	2460094.04	3.23	2461910.93	3.45	2463727.81	3.67	0.95	20244.924	128.7559	16.0378	2023 May 29	2028 May 19	2033 May 10
HD 142091	b	2459098.22	32.95	2460383.06	46.94	2461667.89	61.15	0.86	661.820	88.0362	2.2080	2020 Sep 5	2024 Mar 13	2027 Sep 19
HD 145428	*	2462668.38	397.89	2468280.63	744.03	2473892.87	1090.24	0.38	4043.203	249.4931	14.9158	2030 Jun 15	2045 Oct 27	2061 Mar 9
HD 148284	*	2458524.00	0.19	2458863.30	0.22	2459202.60	0.24	1.10	5465.489	14.7810	1.0175	2019 Feb 9	2020 Jan 14	2020 Dec 19
HD 152581	b	2458997.97	25.32	2459684.46	29.86	2460370.94	34.45	1.48	587.046	77.2530	1.8274	2020 May 28	2022 Apr 14	2024 Mar 1
HD 163607	b	2458398.49	0.41	2458473.71	0.42	2458548.93	0.43	9.42	5468.759	5.3829	0.3706	2018 Oct 6	2018 Dec 21	2019 Mar 6
⋯	c	2459545.27	17.76	2460817.26	22.21	2462089.25	26.66	0.34	4911.309	38.6675	2.5324	2021 Nov 26	2025 May 21	2028 Nov 13
⋯	d	2486985.03	55697.98	2523485.03	69120.33	2559985.03	82553.73	0.05	4403.954	95.3278	5.9325	2097 Jan 11	2196 Dec 18	2296 Nov 24
HD 180053	b	2458409.70	7.29	2458623.42	7.73	2458837.13	8.19	2.51	923.284	34.8194	1.0267	2018 Oct 18	2019 May 19	2019 Dec 19
HD 180902	b	2458519.95	9.27	2459030.83	10.59	2459541.71	11.94	1.44	907.231	55.2221	1.6146	2019 Feb 5	2020 Jun 30	2021 Nov 23
⋯	*	2458811.85	432.62	2464687.86	864.08	2470563.88	1492.06	0.41	854.855	89.2750	2.5361	2019 Nov 24	2035 Dec 26	2052 Jan 27
⋯	c	2458407.32	7.73	2458423.22	7.73	2458439.13	7.73	19.37	193.241	13.1158	0.1792	2018 Oct 15	2018 Oct 31	2018 Nov 16
HD 181342	b	2458512.87	29.15	2459077.01	32.59	2459641.16	36.15	1.38	671.517	62.1357	1.5694	2019 Jan 29	2020 Aug 15	2022 Mar 2
HD 185269[a]	b	2458397.66	0.12	2458404.50	0.12	2458411.34	0.12	13.79[a]	4158.104	6.4653	0.3906	2018 Oct 6	2018 Oct 13	2018 Oct 19
HD 192699	b	2458513.21	8.92	2458854.15	9.70	2459195.09	10.50	2.16	786.785	47.6008	1.2987	2019 Jan 29	2020 Jan 5	2020 Dec 11
HD 193342	*	2462813.37	14955.48	2472466.91	30914.85	2482120.44	46834.52	0.27	4388.284	227.6026	14.1406	2030 Nov 7	2057 Apr 13	2083 Sep 17
HD 195787	*	2459422.83	1.40	2461332.09	1.68	2463241.35	2.00	1.02	12042.169	82.6617	8.1740	2021 Jul 27	2026 Oct 18	2032 Jan 9
HD 196645	b	2458473.62	11.52	2458602.56	11.90	2458731.50	12.29	3.38	1484.883	26.7608	0.9928	2018 Dec 21	2019 Apr 29	2019 Sep 5
HD 200964	b	2458926.10	21.24	2459532.43	24.92	2460138.76	28.65	1.61	652.605	65.1233	1.6221	2020 May 17	2021 Nov 13	2023 Jul 13
⋯	c	2458767.79	28.41	2459620.25	35.37	2460472.71	42.41	1.01	673.304	95.5130	2.4156	2019 Oct 11	2022 Feb 9	2024 Jun 11
HD 206610	b	2458959.86	19.45	2459633.01	22.42	2460306.17	25.46	1.61	409.932	89.3480	1.7730	2020 Apr 20	2022 Feb 22	2023 Dec 27
HD 207077	b	2458749.90	35.94	2459356.21	40.23	2459962.51	44.74	1.10	1049.793	72.6645	2.2804	2019 Sep 23	2021 May 21	2023 Jan 18
HD 210702	b	2458551.16	8.31	2458905.26	8.89	2459259.36	9.48	2.04	643.242	55.5278	1.3734	2019 Mar 8	2020 Feb 25	2021 Feb 13
HD 212771	b	2458403.22	15.54	2458783.94	16.78	2459164.67	18.04	2.19	541.166	58.8900	1.3387	2018 Oct 11	2019 Oct 27	2020 Nov 11
HD 214823	*	2459227.73	4.42	2461081.61	5.87	2462935.49	7.37	0.36	2962.866	38.0524	1.9643	2021 Jan 13	2026 Feb 10	2031 Mar 9
HD 4917	b	2458760.37	14.45	2459160.92	15.97	2459561.46	17.50	1.96	628.655	65.7449	1.6080	2019 Oct 3	2020 Nov 7	2021 Dec 12
⋯	c	2459102.46	308.26	2459923.50	319.62	2460744.55	331.14	2.16	640.833	52.9620	1.3076	2020 Sep 9	2022 Dec 10	2025 Mar 10
⋯	d	2459441.36	704.84	2460534.02	741.14	2461626.68	777.38	0.85	669.968	112.9123	2.8488	2021 Aug 14	2024 Aug 11	2027 Aug 9

Notes. Columns 1 and 2 list the star and companion for which transit parameters are computed. A * symbol indicates a stellar companion rather than a planetary companion. Columns 3–8 list the next three transit times and uncertainties after 2018 October 1 in BJD. Columns 9–12 list transit probabilities, depths, durations, and ingress/egress durations, respectively. The transit probabilities are calculated purely from the best-fit radial velocity parameters. We have performed a literature search for those planets with transit probabilities greater than 10%; those that are known to transit or not transit are marked accordingly. Finally, columns 13–15 list the date of the next three transits in yyyy mm dd format (UTC) for easy reference.

[a] Planet is known to not transit.

[b] Planet is known to transit.

(This table is available in machine-readable form.)

$$\Delta\tau_{12} = \frac{PR_{\rm p}}{\pi a} \quad (5)$$

and can be found in columns 11 and 12. We note that the duration equations have been simplified to assume a circular orbit and exclude grazing transits, which are acceptable for first-order calculations. Finally, the three transit times given in columns 3, 5, and 7 are listed again in YYYY MM DD format (UTC) for quick reference.

While the large majority of planets have probabilities 1%–2%, we highlight three planets with transit probabilities greater than 9%: HD 102956 b (26.16%), HD 180902 c (19.37%), and HD 163607 b (9.55%).[14] These are all planets with periods less than about 75 days, relatively short for evolved stars of intermediate mass. With the exception of HD 180902 c, which is a large hot Neptune candidate, they also have predicted depths of ∼800 ppm or more, which makes these more amenable for ground-based observations than the other planets. Although 800 ppm is still a challenge for ground-based observing, it has been demonstrated on midclass telescopes with diffuser-assisted photometry (Stefansson et al. 2017). As short-period RV planets, their periods are more tightly constrained, and so transit time uncertainties are relatively small (≪1 day, with the exception of HD 180902 c). We emphasize that the majority of the planets around subgiants have semimajor axes of 1 au or more, which in combination with the large stellar radii leads to long transit durations, small transit depths, and lower transit probabilities.[15] In addition, many of the uncertainties in the midtransit times are on the order of 10 days (anywhere from 13 days to 150 days), which makes hunting for them with ground-based telescopes difficult. These factors are what make these planets more amenable to a space-based survey like *TESS*, which may incidentally catch a single transit for one of these planets.

Refitting each known planet as we did means that Table 3, which contains the best-fit orbital parameters for all CPS subgiant stars with known planets, lists the most precise and up-to-date orbital solutions for these planets.

7. Summary and Conclusion

In this work, we presented the discovery of 15 new planetary signals around subgiant stars, 8 of which are planet candidates requiring further observations, increasing the number of known RV planets around subgiants by ∼15% (25% including the candidates). Of special importance are possibly the first three-planet systems around subgiant stars, HD 163607 and HD 4917. As observations on subgiants continue and more long-period planets are discovered, these systems will be useful in determining how multiplanet systems evolve as their host star leaves the main sequence. We lastly note several stellar companions of brown dwarfs to nearly solar mass size and provide orbital parameters for these systems as well.

In this work, we have calculated transit parameters (transit times, probabilities, depths, and durations, see Table 5) for all known planets around CPS subgiant stars ($3 < \log g < 4$). We find that three planets have relatively high transit probabilities ($\gtrsim 10\%$). These planets have the best chance of having a transit observed from a ground-based telescope. The remaining 50 planets in general all have lower transit probabilities (1%–2%), longer transit durations (∼50 hr), smaller transit depths (of order 500 ppm), and more uncertain transit times (tens of days). The combination of these factors indicates that these are challenging to observe from the ground, but instead will make good targets for future space-based missions like *TESS*. In predicting transit parameters, we have made use of additional RV observations since the planets' initial discoveries and updated stellar parameters to refit all planets, resulting in updated orbital parameters for all planets (Table 3).

ORCID iDs

Jacob K. Luhn ⓘ https://orcid.org/0000-0002-4927-9925
Fabienne A. Bastien ⓘ https://orcid.org/0000-0002-7243-1921
Jason T. Wright ⓘ https://orcid.org/0000-0001-6160-5888
Andrew W. Howard ⓘ https://orcid.org/0000-0001-8638-0320
Howard Isaacson ⓘ https://orcid.org/0000-0002-0531-1073

References

Baines, E. K., Armstrong, J. T., & van Belle, G. T. 2013, ApJL, 771, L17
Barnes, J. W. 2007, PASP, 119, 986
Bastien, F. A., Stassun, K. G., & Pepper, J. 2014, ApJL, 788, L9
Beatty, T. G., Stevens, D. J., Collins, K. A., et al. 2017, AJ, 154, 25
Borucki, W. J., Koch, D., Basri, G., et al. 2010, Sci, 327, 977
Borucki, W. J., Koch, D. G., Basri, G., et al. 2011, ApJ, 736, 19
Bowler, B. P., Johnson, J. A., Marcy, G. W., et al. 2010, ApJ, 709, 396
Brewer, J. M., Fischer, D. A., Basu, S., Valenti, J. A., & Piskunov, N. 2015, ApJ, 805, 126

---

[14] We have not included HD 93396 (KELT-11), which we list as having a 26% transit probability, because it is known to transit and was in fact discovered via transits (Pepper et al. 2017). We have also excluded HD 88133 b, which has transit probability 22.89% as it has been found to be nontransiting (Piskorz et al. 2016). Additional planets excluded from this list as they have been found to be nontransiting include HD 185269 b (Johnson et al. 2006; Moutou et al. 2006) with 13% transit probability, and HD 38529 b (Henry et al. 2013) with 13% transit probability.

[15] The increased stellar radii actually helps to inflate the transit probabilities, but the large separations ultimately account for the low probabilities.

Luhn et al.

Brewer, J. M., Fischer, D. A., Valenti, J. A., & Piskunov, N. 2016, ApJS, 225, 32

Brewer, J. M., Fischer, D. A., Valenti, J. A., & Piskunov, N. 2017, ApJS, 230, 12

Bryan, M. L., Knutson, H. A., Howard, A. W., et al. 2016, ApJ, 821, 89

Butler, R. P., Marcy, G. W., Williams, E., et al. 1996, PASP, 108, 500

Butler, R. P., Vogt, S. S., Laughlin, G., et al. 2017, AJ, 153, 208

Butler, R. P., Wright, J. T., Marcy, G. W., et al. 2006, ApJ, 646, 505

Chen, J., & Kipping, D. 2017, ApJ, 834, 17

Ciceri, S., Lillo-Box, J., Southworth, J., et al. 2015, A&A, 573, L5

Collins, K. A., Eastman, J. D., Beatty, T. G., et al. 2014, AJ, 147, 39

Dawson, R. I., & Fabrycky, D. C. 2010, ApJ, 722, 937

Díaz, R. F., Ségransan, D., Udry, S., et al. 2016, A&A, 585, A134

Diego, F., Charalambous, A., Fish, A. C., & Walker, D. D. 1990, Proc. SPIE, 1235, 562

Endl, M., Kürster, M., & Els, S. 2000, A&A, 362, 585

Fischer, D. A., & Valenti, J. 2005, ApJ, 622, 1102

Ghezzi, L., Montet, B. T., & Johnson, J. A. 2018, ApJ, 860, 109

Giguere, M. J., Fischer, D. A., Howard, A. W., et al. 2012, ApJ, 744, 4

Giguere, M. J., Fischer, D. A., Payne, M. J., et al. 2015, ApJ, 799, 89

Harakawa, H., Sato, B., Fischer, D. A., et al. 2010, ApJ, 715, 550

Henry, G. W., Kane, S. R., Wang, S. X., et al. 2013, ApJ, 768, 155

Howard, A. W., Johnson, J. A., Marcy, G. W., et al. 2010, ApJ, 721, 1467

Howard, A. W., Johnson, J. A., Marcy, G. W., et al. 2011, ApJ, 726, 73

Huber, D., Chaplin, W. J., Christensen-Dalsgaard, J., et al. 2013, ApJ, 767, 127

Ida, S., & Lin, D. N. C. 2004, ApJ, 604, 388

Isaacson, H., & Fischer, D. 2010, ApJ, 725, 875

Johnson, J. A., Aller, K. M., Howard, A. W., & Crepp, J. R. 2010a, PASP, 122, 905

Johnson, J. A., Butler, R. P., Marcy, G. W., et al. 2007a, ApJ, 670, 833

Johnson, J. A., Clanton, C., Howard, A. W., et al. 2011, ApJS, 197, 26

Johnson, J. A., Fischer, D. A., Marcy, G. W., et al. 2007b, ApJ, 665, 785

Johnson, J. A., Howard, A. W., Bowler, B. P., et al. 2010b, PASP, 122, 701

Johnson, J. A., Marcy, G. W., Fischer, D. A., et al. 2006, ApJ, 652, 1724

Johnson, J. A., Morton, T. D., & Wright, J. T. 2013, ApJ, 763, 53

Johnson, J. A., & Wright, J. T. 2013, arXiv:1307.3441

Jones, H. R. A., Paul Butler, R., Marcy, G. W., et al. 2002, MNRAS, 337, 1170

Jones, M. I., Jenkins, J. S., Brahm, R., et al. 2016, A&A, 590, A38

Kane, S. R., Mahadevan, S., von Braun, K., Laughlin, G., & Ciardi, D. R. 2009, PASP, 121, 1386

Kaufer, A., Stahl, O., Tubbesing, S., et al. 1999, Msngr, 95, 8

Lloyd, J. P. 2011, ApJL, 739, L49

Lloyd, J. P. 2013, ApJL, 774, L2

Morton, T. D., Bryson, S. T., Coughlin, J. L., et al. 2016, ApJ, 822, 86

Moutou, C., Loeillet, B., Bouchy, F., et al. 2006, A&A, 458, 327

Noguchi, K., Aoki, W., Kawanomoto, S., et al. 2002, PASJ, 54, 855

Otor, O. J., Montet, B. T., Johnson, J. A., et al. 2016, AJ, 152, 165

Peek, K. M. G., Johnson, J. A., Fischer, D. A., et al. 2009, PASP, 121, 613

Pepper, J., Rodriguez, J. E., Collins, K. A., et al. 2017, AJ, 153, 215

Piskorz, D., Benneke, B., Crockett, N. R., et al. 2016, ApJ, 832, 131

Quinn, S. N., White, T. R., Latham, D. W., et al. 2015, ApJ, 803, 49

Ramsey, L. W., Adams, M. T., Barnes, T. G., et al. 1998, Proc. SPIE, 3352, 34

Ricker, G. R., Winn, J. N., Vanderspek, R., et al. 2014, Proc. SPIE, 9143, 914320

Robinson, S. E., Laughlin, G., Vogt, S. S., et al. 2007, ApJ, 670, 1391

Rowe, J. F., Bryson, S. T., Marcy, G. W., et al. 2014, ApJ, 784, 45

Sato, B. 2005, JKAS, 38, 315

Sato, B., Izumiura, H., Toyota, E., et al. 2008, PASJ, 60, 539

Sato, B., Omiya, M., Harakawa, H., et al. 2012, PASJ, 64, 135

Schlaufman, K. C., & Winn, J. N. 2013, ApJ, 772, 143

Seager, S. 2010, Exoplanets (Tucson, AZ: Univ. Arizona Press)

Seager, S., & Mallén-Ornelas, G. 2003, ApJ, 585, 1038

Seagroves, S., Harker, J., Laughlin, G., Lacy, J., & Castellano, T. 2003, PASP, 115, 1355

Stefansson, G., Mahadevan, S., Hebb, L., et al. 2017, ApJ, 848, 9

Stello, D., Huber, D., Grundahl, F., et al. 2017, MNRAS, 472, 4110

Stevens, D. J., & Gaudi, B. S. 2013, PASP, 125, 933

Tokovinin, A., Fischer, D. A., Bonati, M., et al. 2013, PASP, 125, 1336

Tull, R. G. 1998, Proc. SPIE, 3355, 387

Tull, R. G., MacQueen, P. J., Sneden, C., & Lambert, D. L. 1995, PASP, 107, 251

Valenti, J. A., Fischer, D., Marcy, G. W., et al. 2009, ApJ, 702, 989

Villaver, E., & Livio, M. 2009, ApJL, 705, L81

Vogt, S. S. 1987, PASP, 99, 1214

Wang, S. X., Wright, J. T., Cochran, W., et al. 2012, ApJ, 761, 46

Wenger, M., Ochsenbein, F., Egret, D., et al. 2000, A&AS, 143, 9

Wittenmyer, R. A., Endl, M., Cochran, W. D., Levison, H. F., & Henry, G. W. 2009, ApJS, 182, 97

Wittenmyer, R. A., Horner, J., Tinney, C. G., et al. 2014, ApJ, 783, 103

Wittenmyer, R. A., Horner, J., Tuomi, M., et al. 2012, ApJ, 753, 169

Wittenmyer, R. A., Johnson, J., Wang, L., & Endl, M. 2011, in AIP Conf. Ser. 1331, Planetary Systems beyond the Main Sequence, ed. S. Schuh, H. Drechsel, & U. Heber (Melville, NY: AIP), 117

Wright, J. T. 2005, PASP, 117, 657

Wright, J. T., Upadhyay, S., Marcy, G. W., et al. 2009, ApJ, 693, 1084